HEAT TRANSFER-ASIAN RESEARCH

Online ISSN:1523-1496; Publisher – Wiley (USA).

(*Accepted May 13^TH 2019*)

COMPUTATIONAL FLUID DYNAMIC AND THERMAL STRESS ANALYSIS OF COATINGS FOR HIGH-TEMPERATURE CORROSION PROTECTION OF AEROSPACE GAS TURBINE BLADES

Ali Kadir[1]
[1] *Department of Mechanical and Aeronautical Engineering, Salford University, Salford, M54WT,* ***UK.***
A.Kadir@salford.ac.uk

O. Anwar Bég[2]
[2] *Department of Mechanical and Aeronautical Engineering, Salford University, Salford, M54WT,* ***UK.***
O.A.Beg@salford.ac.uk

Mohammed El Gendy[3]
[3] *Aerospace Engineer, Lufthansa Technik Malta (LTM), Malta Intl. Airport Hal Farrug Road Luqa LQA 3079,*
MALTA.
mgendy93@gmail.com

Tasveer A. Bég[4]
[4]*Computational Mechanics and Renewable Energy Research, Israfil House, Dickenson Rd., Manchester,* ***UK.***
tasveerabeg@gmail.com

MD. Shamshuddin[5*]
[5]*Department of Mathematics, Vaagdevi College of Engineering, Warangal, Telangana,* ***INDIA.***
shammaths@gmail.com

****Corresponding author- email: shammaths@gmail.com; shamshuddin_md@vaagdevi.edu.in***
Orchid Number: ***0000-0002-2453-8492***

ABSTRACT

The current investigation presents detailed finite element simulations of coating stress analysis for a 3-dimensional, 3-layered model of a test sample representing a typical gas turbine component. Structural steel, Titanium alloy and Silicon Carbide are selected for main inner, middle and outermost layers respectively. ANSYS is employed to conduct three types of analysis- static structural, thermal stress analysis and also computational fluid dynamic erosion analysis (via ANSYS FLUENT). The specified geometry which corresponds to corrosion test samples exactly is discretized using a body-sizing meshing approach, comprising mainly of tetrahedron cells. Refinements were concentrated at the connection points between the layers to shift the focus towards the static effects dissipated between them. A detailed grid independence study is conducted to confirm the accuracy of the selected mesh densities. The momentum and energy equations were solved, and the viscous heating option was applied to represent improved thermal physics of heat transfer between the layers of the structures. A discrete phase model (DPM) in ANSYS FLUENT was employed which allows for the injection of continuous uniform air particles onto the model, thereby enabling an option for calculating the corrosion factor caused by hot air injection. Extensive visualization of results is provided. The simulations show that ceramic (silicon carbide) when combined with titanium clearly provide good thermal protection; however, the ceramic coating is susceptible to cracking and the titanium coating layer on its own achieves significant thermal resistance. Higher strains are computed for the two-layer model than the single layer model (thermal case). However even with titanium only present as a coating the maximum equivalent elastic strain is still dangerously close to the lower edge. Only with the three-layer combined ceramic and titanium coating model is the maximum equivalent strain *pushed deeper towards the core central area*. Here the desired effect of restricting high stresses to the strongest region of the gas turbine blade model is achieved, whereas in the other two models, lower strains are produced in the core central zones. Generally, the CFD analysis reveals that maximum erosion rates are confined to a *local zone on the upper face of the three-layer system* which is in fact the sacrificial layer (ceramic coating). The titanium is not de-bonded or damaged which is essential for creating a buffer to the actual blade surface and mitigating penetrative corrosive effects. The present analysis may further be generalized to consider three-dimensional blade geometries and corrosive chemical reaction effects encountered in gas turbine aero-engines.

Key words: *Thermal coating; Silicon Carbide ceramic; ANSYS; Finite element stress analysis; CFD (computational fluid dynamics); mesh density; total deformation; erosion.*

1. INTRODUCTION

Modern gas turbine blades experience significant thermal loading during expected life cycles. Temperatures can attain in excess of 1000 °C. It is therefore necessary to coat the blades with thermal barrier coatings (TBCs) which also provide protection from oxidation, corrosion, debris impact and thereby mitigate possible failures [1-4]. Additionally, there are high centrifugal stresses and shock loadings present. Many excellent studies have been conducted on the performance of TBCs in real systems. It has been established that temperature decay across TBCs is a function of material and geometrical properties of the TC (a ceramic top-coat) layer, in particular the thickness of the layer and thermal conductivity [5]. Ceramics have emerged as the most resilient to high temperature conditions, although cracking may occur, and other discontinuities may appear under long duration exposure to corrosive gases. Once coatings are compromised these may lead to thermal fracture, yield behaviour and even creep failures. A critical aspect of sustaining good thermal protection is the interfacial bonding between layers and in particular the bonding integrity between the blade and the first layer of coating. Control of oxidation is also a very significant aspect of mitigating corrosion damage. Echsler et al., [6] investigated bond coat oxidation in gas turbine thermal coatings between 950 and 1100 °C using scanning electron microscopy (SEM), determining maximum crack lengths under long duration. Patnaik et al., [7] studied experimentally the oxidation, thermal fatigue (TF) and inter-diffusion in a directionally solidified nickel-based superalloy with a diffusion aluminide coating, noting the propagation of extensive cracks in the coating associated with internal cooling passages along the blade. Many excellent works up to 1989 were reviewed lucidly by Mévrel [8]. Yoshiba [9] reported on high temperature corrosive thermal creep rupture tests for many nickel-base superalloys and several plasma spray coating systems. He considered cases where a ceramic top coat is present and absent showing significant corrosion-induced creep rupture strength degradation associated with coating bonding defects. Yoshiba et al., [10] performed high-temperature oxidation and hot corrosion tests at 800 to 1100 °C under isothermal and thermal-cycle conditions for Y_2O_3-stabilized zirconia (YSZ) and CaO-SiO_2-ZrO_2 (C_2S-CZ) ceramic topped coatings with a focus of failure. They observed that spalling arises more freely in the YSZ-TBC system owing to localized oxidation along the ceramic top coat/metallic (NiCrAlY) bond coat interface. They also identified important hot corrosion mechanisms and the synthesis of a new phase layer composed of with more corrosive species (oxygen) at the inner region of the ceramic top coat. Bai et al., [11] reported on detailed tests on the resistance of various coatings on superalloy IN-738LC to high temperature oxidation and corrosion. They showed that at temperatures exceeding 850 °C, aluminized–chromized coating layers are most easily compromised against oxidation and that this is attributable to the spalling or cracking of the oxide scales. However, the aluminized coatings were found to produce better protection under hot corrosion conditions compared with siliconized coatings which exhibit excessive brittle fracture caused by thermal shock and are inadequate for superalloy IN-738-LC. Koo et al., [12] also investigated coating behaviour during high temperature oxidation and hot corrosion of superalloy IN-738LC with three aluminized coatings (simple aluminized, Rhodium-electroplated aluminized and Palladium-electroplated aluminized coatings) also conducting Vickers hardness tests (for micro-hardness). They found that Rh-plated aluminized performs the best followed by simple aluminized, Pd-plated aluminized, and uncoated superalloy IN-738LC samples. Sumner et al., [13], simulated in careful experiments the influence of fly ash, gas moisture and high gas temperatures on the alkali sulphate induced hot corrosion of CM247LC, Haynes 230, IN939 and IN728LC gas turbine super alloys. They identified Type I (sulphidation and internal damage), type II (pitting) and mixed mode hot corrosion under different thermal loadings and furthermore that hot corrosion damage is decreased with the presence of fly ash. Higher chromium content alloys were observed to achieve better resilience compared with high Aluminium content CM247LC super alloys and showed better oxidation resistance. Oska et al., [14] investigated the performance of thermal spray NiCr (51Ni-46Cr-2Si-1Fe) and FeCr (Fe-19Cr-9W-7Nb-4Mo-5B-2C-2Si-1Mn) powders on gas turbine blades using HVOFGF (High-Velocity Oxygen Fuel Gas-Fuelled) and HVOFLF (High-Velocity Oxygen Fuel Liquid-Fuelled) systems under high temperature corrosion conditions. Khan et al., [15] described corrosion kinetics, surface morphology and X-ray analysis of Inconel 617 super alloy under high temperatures. They observed that the Vanadium Oxide (V_2O_5) component in the salt mixture exerts a significant role in corrosion degradation of the super allow and accelerates hot corrosion effects and that better protection is achieved with lower concentrations.

The above studies generally confirmed that chemical constitution of the super alloy and thermal insulation capability of the coatings both have a critical role in the impact of hot corrosion on long-term gas turbine blade performance. Ceramics tend to perform best; however, they are prone to fracture and delamination. Thermal mismatch stress within the coatings can be elevated if bonding is not sustained. There is evidently a balance between the thermal insulation capability and thermal stress level and a crucial engineering task is to accurately determine the optimum thermal coating thickness. This presents an on-going challenge for corrosion engineers which can be greatly assisted with numerical simulation. Computational mechanics provides a safe, easily-controlled, relatively inexpensive methodology for mimicking realistic high temperature corrosion conditions and evaluating the TBC protection performance of an unlimited number of coating materials for super alloys. This can therefore allow protective layers to be optimized in the design process and therefore improve the efficiency of gas turbine blade systems. Although the conventional TBC system is composed of a load carrying substrate, a ceramic top-coat (TC), a metallic bond-coat (BC), and the thermally grown oxide (TGO) that forms between TC and BC, modifications to these structures can be easily attained with computational simulation. Of course, data must be extracted from actual tests and material properties must be representative of high thermal conditions. We further note that a dilemma faces modern gas turbine design. Sustaining coating integrity for a TBC is more problematic than pure metallic coatings due to the considerable *transition* in properties from the metallic substrate to the ceramic coating. This issue is further amplified since TBCs attain the greatest efficiency benefit at the highest operating temperatures, where TBC failure is most likely to cause unacceptable component damage. Thus, while coatings with even lower conductivity may be possible, the high variability of TBC thermal cycle life implies that the implementation of these coatings to their full potential will depend on their susceptibility to failure. To address these (and other) aspects many researchers have developed robust numerical models for high temperature corrosive stress behaviour of TBCs. The most popular approach for static/thermal stress analysis in gas turbine blade systems is the finite element method (FEM) which is available commercial codes (ANSYS, ADINA, ABAQUS, NASTRAN etc). Many non-commercial finite element simulations of the high temperature corrosion response of gas turbine systems have also been developed. Bäker [16] presented detailed two-dimensional finite element simulations of crack initiation and propagation at the interface between the TGO and the TBC in thermal barrier coatings. He showed that cracks in the peak position propagate in mode II for cases where even with TGO thickness is small and achieve lower stress relaxation than valley cracks. Chen [17] examined the influence of foreign object damage (FOD) and mechanical erosion in failure analysis of thermal barrier coatings, using a novel impact scaling analysis and a moving finite element method. He studied in detail the effects of particle size, velocity, temperature and TBC composition and showed that transient stresses mobilize the propagation of cracks whereas residual stresses dictate the delamination of the coating. Yang et al., [18] investigated with finite element analysis the cyclic high thermal loading effects on ceramic coated turbine blades, identifying critical zones using the maximum principal stress criterion and showing that with sustained excessive thermal stresses there is significant reduction in thermal fatigue life. Mohamed [19] employed ABAQUS finite element software to simulate thermal coating performance with four approaches, namely TGO thickness computation, elasticity and creep effect analysis, a coupled oxidation constitutive approach and fracture mechanics. He evaluated the local von Mises stress distribution on each layer in of the three layers of the coating, validating against previous experimental results. Fan et al., [20] examined the double-ceramic-layer (DCL) thermal coating system using a virtual crack closure interfacial element method, computing energy release rates for interfacial delamination. They conducted a parametric investigation of geometrical and material parameter influence and showed that it is possible to determine an optimal thickness ratio of outer to inner ceramic layers. They further showed that local separation between two ceramic layers facilitates the onset of delamination and assists in it spreading at the inner coating and lower layer interface. Xu et al., [21] presented detailed simulations aimed at establishing the contribution of mixed oxides on structural integrity and interfacial failure mechanisms in a thermal barrier coating system, observing that large mixed oxide growth rates encourage the synthesis and subsequent propagation of interface cracks leading to ceramic coating de-bonding. Gupta et al., [22] described both experimental (laser flash tests) and finite element computations focused on elucidating the performance of zirconia coatings in thermal protection of gas turbine components. They found that low thermal conductivity coatings achieve greater resistance when large globular pores and connected cracks within the coating microstructure are present. Busso et al., [23] considered the effect of the oxidation induced degradation of a plasma-sprayed thermal barrier coating (PS-TBC) system on the local ceramic–metal interfacial stresses using a parametric unit cell finite element code. They noted that local morphology of the oxidized interface, sintering of the ceramic coating, stress relaxation effects due to creep and the thickness of the thermally grown oxide (of the order of micrometers) all contribute substantially to the local stresses responsible for mesoscopic crack nucleation and growth. These studies were confined to thermo-mechanical stress analysis and did not consider the corrosive gas environment. To simulate the total thermo-structural and fluid dynamics problem, a CFD approach is generally required. The temperature field generated by computational flow simulation provides a more accurate thermal loading input for the coatings. Zhu et al., [24] were among the first researchers to employ a coupled thermal stress and thermofluid simulation in high temperature gas turbine corrosion analysis. They employed a three-dimensional finite element model of multi-layered coated turbine blade with a conjugate heat transfer analysis and decoupled thermal-stress computation procedure. They computed the thermal flow field impinging on the coating with three turbulence models (RNG k-ε, realizable k-ε and SST k-ω model), obtaining the best correlation with experimental high temperature data for temperature and pressure distribution with the realizable k-ε turbulence model. Their simulations succinctly demonstrated that improved thermal protection (insulation performance) is achieved at the blade leading and trailing edges, that specific danger zones susceptible to failure exist and that greater stress levels are induced in the ceramic layer relative to the bond coating (leading to possible spalling). Tang et al., [25] performed a similar analysis to [24] although they considered a non-uniform temperature distribution along the blade surface and evaluated a leading-edge temperature reaching 1030 °C. They further computed a peak stress of 3.75 GPa located at the center of the blade suction face for TGO and a maximum compressive stress of −3.5 GPa at the leading edge in the cooling stage (a cause of potential failure). Sadowski and Golewski [26] conducted coupled CFD and transient thermal stress analysis in unprotected and thermal barrier coated alloy Inconel 713 up to 1000 °C with 0.5 mm deep coatings. They used ANSYS Fluent code to compute the pressure and thermal fields induced by the combustion gas and ABAQUS to simulate the resulting thermo-structural behaviour in the coated blade. In the current work we employ the ANSYS structural and FLUENT tools to perform computational stress analysis and high temperature flow analysis on bare (unprotected) and titanium or ceramic (SiC) coated gas turbine blade samples. A three-dimensional model is produced in both cases. Body meshing is achieved with tetrahedron cells. A mesh independence study is included to verify the results, which provide a compliment to on-going experimental studies also being undertaken by the authors. Equivalent elastic strain, total deformation, equivalent stress and strain energy fields are computed for all the scenarios examined. The CFD ANSYS Fluent analysis is based on a Discrete Phase Model (DPM) which quite efficiently generates a continuous high temperature corrosive gas stream and permits an assessment of corrosion impact on structural integrity. A viscous heating effect is also included in the CFD analysis to improve the interfacial layer heat transfer prediction. Extensive visualization of results is provided. The simulations show that the different coatings offer mixed benefits for thermal barrier coating protection. These provide a useful compliment to alternative studies of gas turbine film cooling from a purely computational fluid dynamics view point [27, 28] or purely stress analysis view point.

2. COMPUTATIONAL METHODOLOGY

2.1 Computational Structural/Thermo-Structural Analysis

All finite element stress (structural) and fluid dynamics simulations have been executed in the ANSYS Workbench version **16.2** [29, 30]. Here we first elaborate on the stress analysis and in the next section provide details on the CFD analysis. The general methodology is summarized in Figure 1. A three-dimensional model was created using the ANSYS static structural geometry modeller to represent an exact replica of a sample deployed in HVOF (High-Velocity Oxygen Fuel) high temperature corrosion bath experiments [31]. A three-layered domain in (x,y,z) space is created with each layer representing the three main materials of interest, namely a core steel layer, an intermediate Titanium layer and an outer ceramic (Silicon Carbide SiC) layer. The core and outer ceramic layers are plotted in Figures 2 and 3. The inner Titanium (metallic) domain is depicted in Figure 4, measured 20 mm in width and 10 mm in height with the outer domains adding a millimetre depth to this core steel geometry section, respectively. All material parameters (Young modulus, Poisson ratio, coefficient of thermal expansion, density etc) are selected from the engineering data library present in the ANSYS code. Isotropic, homogenous elastic behaviour is assumed.

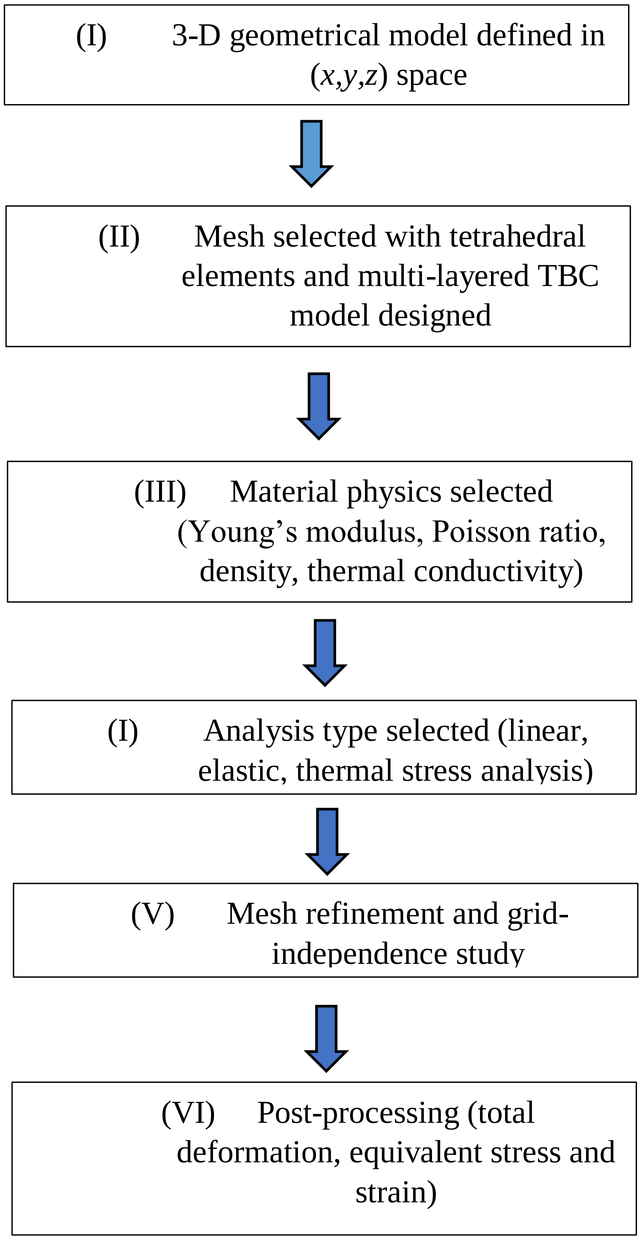

Figure 1. ANSYS finite element stress analysis procedure (CORRECTED FIGURE)

The three-dimensional elasticity equations (equilibrium, constitutive and compatibility) and thermal conduction model is readily available in [30] and not repeated here.

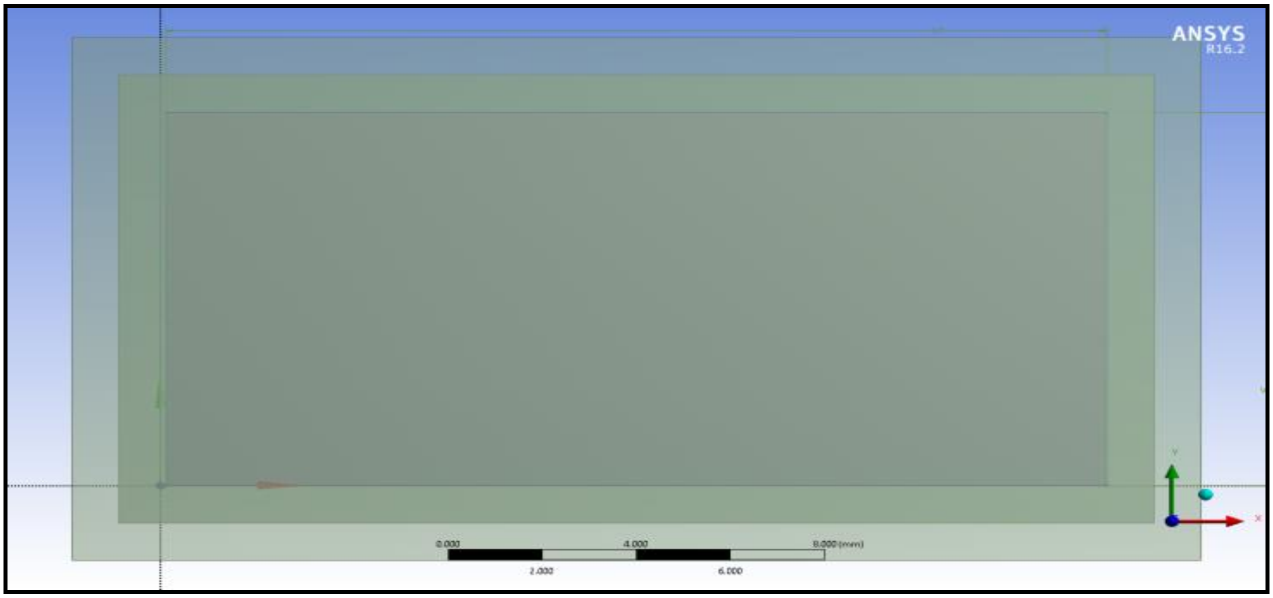

Figure 2. Steel core layer

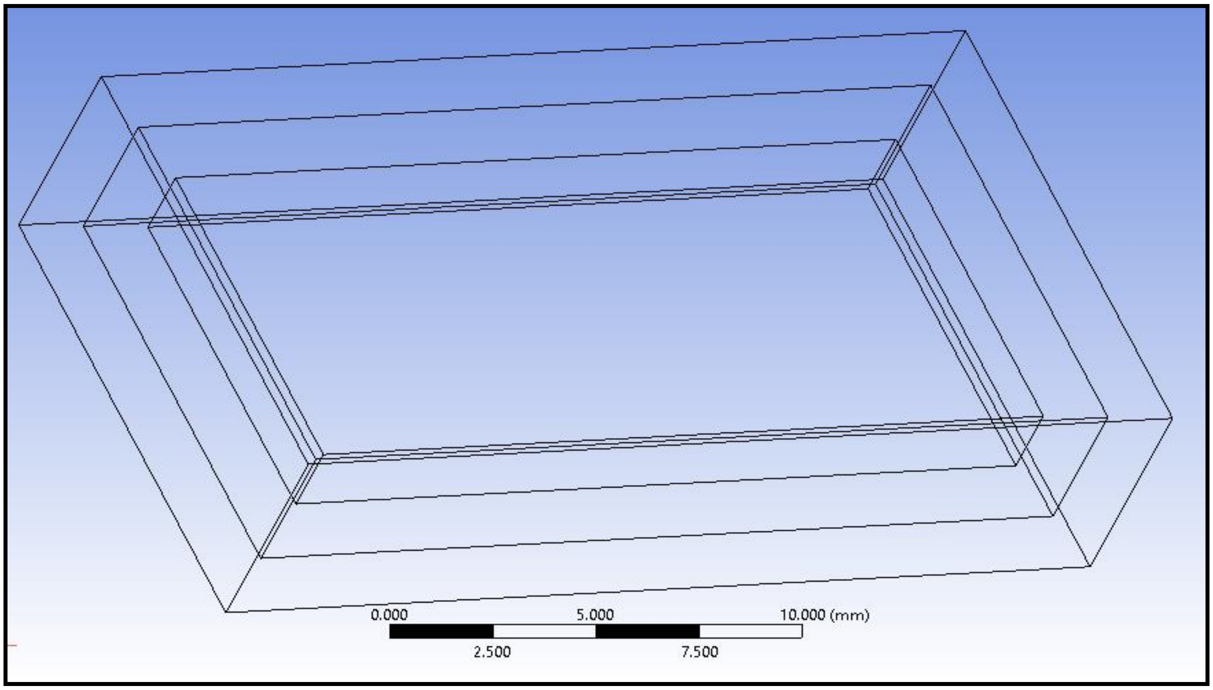

Figure 3. Outer ceramic (SiC) layer

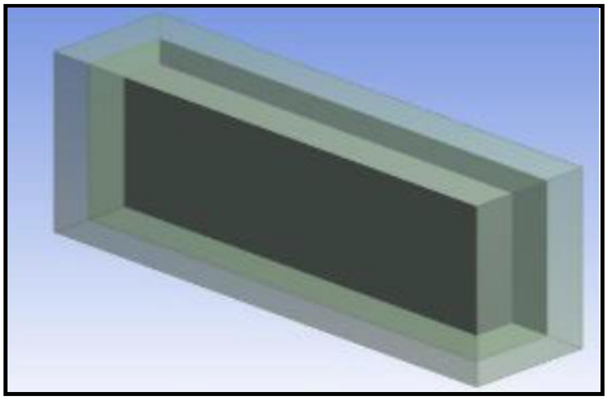

Figure 4. Intermediate Titanium layer

Due to the relatively simple geometry of the blade sample model, a body-sizing meshing approach, compromising mainly of tetrahedron cells, was used to produce efficient meshing which guarantees high accuracy and low computational times. Refinements were concentrated at the connection points between the layers to displace the focus towards the static effects dissipated between them. The cell distribution around the model is shown in Figures 5 and 6. To verify the accuracy of the meshing, a grid-independence study was also conducted for both the structural analysis component and the CFD component. The results are summarized for structural grid independence (deformation analysis) in **Table 1** and the results for CFD mesh independence are given in Figure 7. The grid independency study results indicated that reducing the mesh size by more than half, saved a massive amount of computing time while maintaining the reliability of the results. There is no need to use the densest meshes since these do not modify the results tangibly and intermediate mesh densities achieve grid independence and the requisite accuracy in simulations.

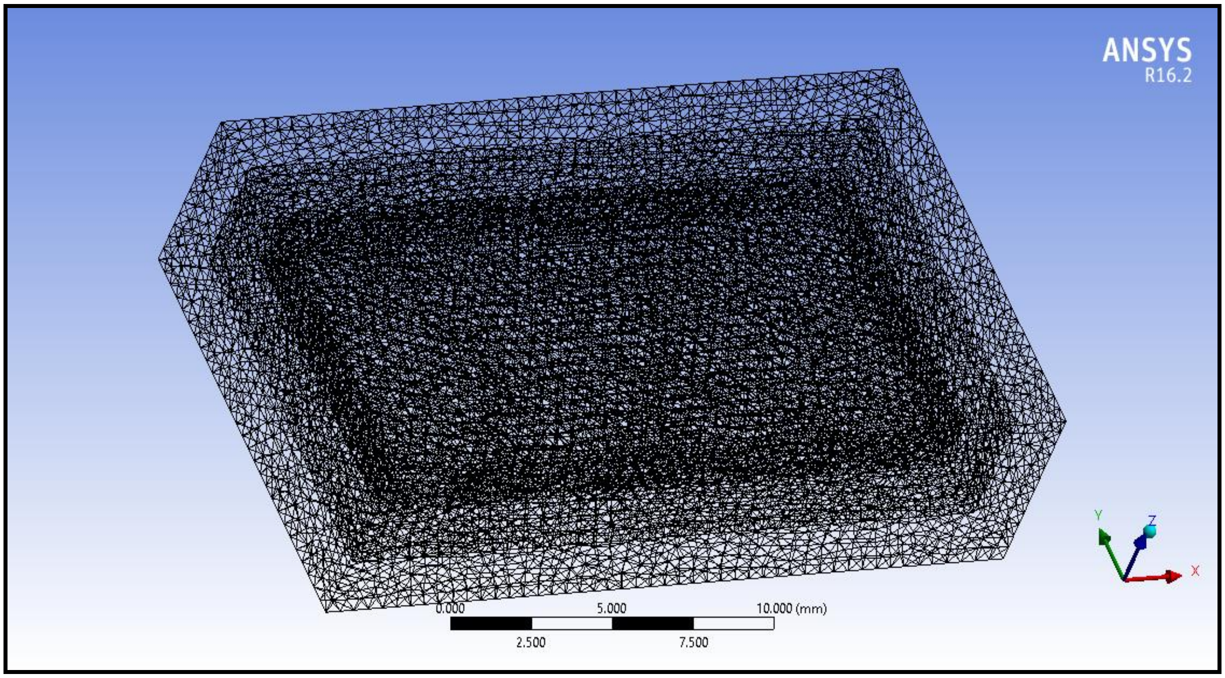

Figure 5. A wireframe rendition of the geometrical multi-layered model.

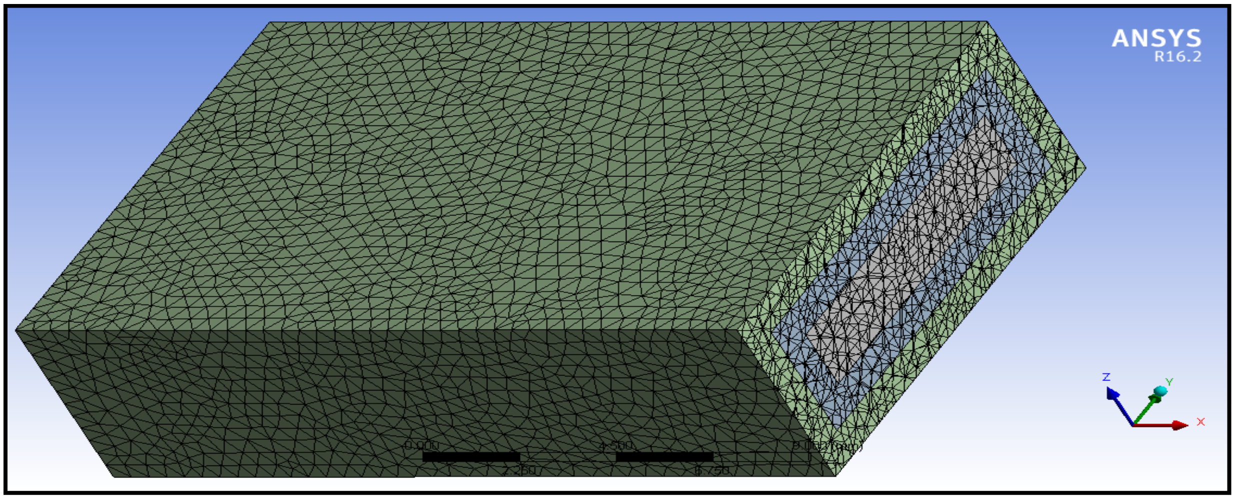

Figure 6. **S**howing a section plane from the mesh produced outlining the refinement between the layers

Table 1. Representation of the effect of mesh density on the simulation values

Mesh	Total no. of cells	Total Deformation (mm)	Computational time (minutes)
Double refinement	1543818	0.24521	90
Original mesh	362018	0.24493	20
Half element sizing	148167	0.24406	5
Quarter element sizing	68256	0.22564	2

The mesh sensitivity was further checked in smaller increments between 80,000 and 120,000 elements. 100,000 elements were found to produce good accuracy with no variation in further mesh refinement and this was adopted as the generic mesh density in the subsequent computations. No modification in total deformation was computed for 110,000 or 120,000 elements. It is therefore feasible to adopt the *100,000 element grid** in the mesh design for the ensuing analysis and the compilation time remains reasonable (4.3 minutes i.e. 258 s). We have included aspects of this commentary in the revised manuscript on Page 11.

Table 2. Further incremental mesh density study

Total no. of cells	Total Deformation (m/s)	Computational time (minutes)
120,000	0.24405	4.6
110,000	0.24405	4.5
100,000*	0.24404	4.3
90, 000	0.24402	4.2
80,000	0.23709	3.5

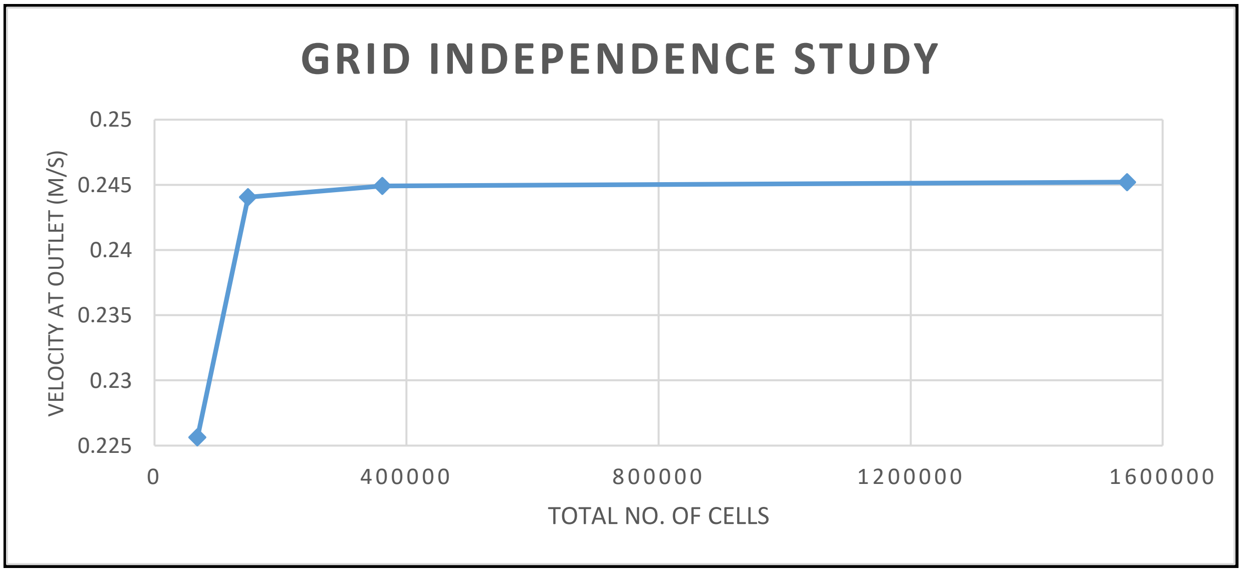

Figure 7. Grid independence study

Following the successful meshing of the models, static and thermal stress simulations are conducted. Two temperatures are considered, 300 K and 1000 K and static loading of up to 1000 N. For the static analysis, the default solver is set the controls for the simulation with a fixed support prescribed at one edge face of the model while subjecting the opposite side to a force of 500 and 1000 N. The software automatically computes the equivalent elastic strain, total deformation, equivalent stress and strain energy. The same process is repeated for the thermal study, with the exception of the inclusion of a tabular thermal condition of 300 and 1000 ℃, while keeping the same outputs. This was followed by duplicating each analysis twice to remove one of the layers each time. This allowed testing of the static and thermal effects on each of the coatings.

2.2 Computational Fluid Dynamics Simulation with ANSYS FLUENT

The meshed model described in Section 2.1 is imported into ANSYS FLUENT to complete the third part of the study, which involved testing the corrosion effects on the model when subjected to the same high temperature conditions. The CFD simulation is inevitably more demanding than the stress analysis. It requires some refinement of the mesh to accommodate for the size of the air particles (hot corrosive air stream) leading to the erosion of the structural coating materials. Chemical reaction effects are neglected. The CFD analysis is used to generate a representative pressure and thermal field. This grid refinement is conducted in the solver phase of the simulation to avoid altering the main mesh of the structure and avoiding errors. The solver is set to include the double precision option to allow a higher accuracy and the parallel processing option is enabled to utilize the power of the multi-core system and the double GPU feature. The effects of gravity are also taken into consideration with $g=-9.81\ m/s^2$ along the z-axis. The standard *K-epsilon* turbulence model was used in this simulation to provide enough refinement in the velocity field and simultaneously avoid excessive compilation times required with alternate turbulence models (e.g. RNG). Other models such as k-omega and Large eddy simulations (LES) are applicable for this type of simulation. These are being considered and are not discussed here. As a first approximation the *K-epsilon* turbulence model is known to provide satisfactory results [30]. Since air is considered, the model constants in the “material physics” option in ANSYS FLUENT are left unaltered. Viscous heating is however switched on to achieve more elegant simulation of the interfacial heat transfer between the layers of the model i.e. at the steel core-Titanium coating and Titanium coating-ceramic interfaces. The energy equation is activated to allow a 3-dimensional heat transfer analysis to be included, based on the classical Fourier law (i.e. thermal relaxation effects are neglected). The DPM option is also mobilized to simulate hot gas injection as a continuous stream of high temperature uniform air particles representing corrosive gas impingement on the blade sample onto the model. This provides a facility for computing the corrosion damage induced by hot gas turbine environments. The particles were set at a speed of 5 m/s with a temperature of 1273.15 K. Boundary conditions where left unaltered with the exception of the inlet with a similar velocity condition to that of the injected particles. A simple scheme with *second order upwind pressure and momentum* was selected and the solution was left to converge for 1000 iterations. The solution converged after 427 iterations within a time frame of 180 minutes. All simulations were performed using a Lenovo Y510p laptop machine with 8 GB of RAM and an Intel® Core i7-4700MQ CPU @ 2.4 GHz processor with a NVidia® 755m gt SLI GPU running on a Windows 10 platform. Comprehensive visualizations of the simulations are described next. The ANSYS FLUENT methodology is summarized in Figure. 8.

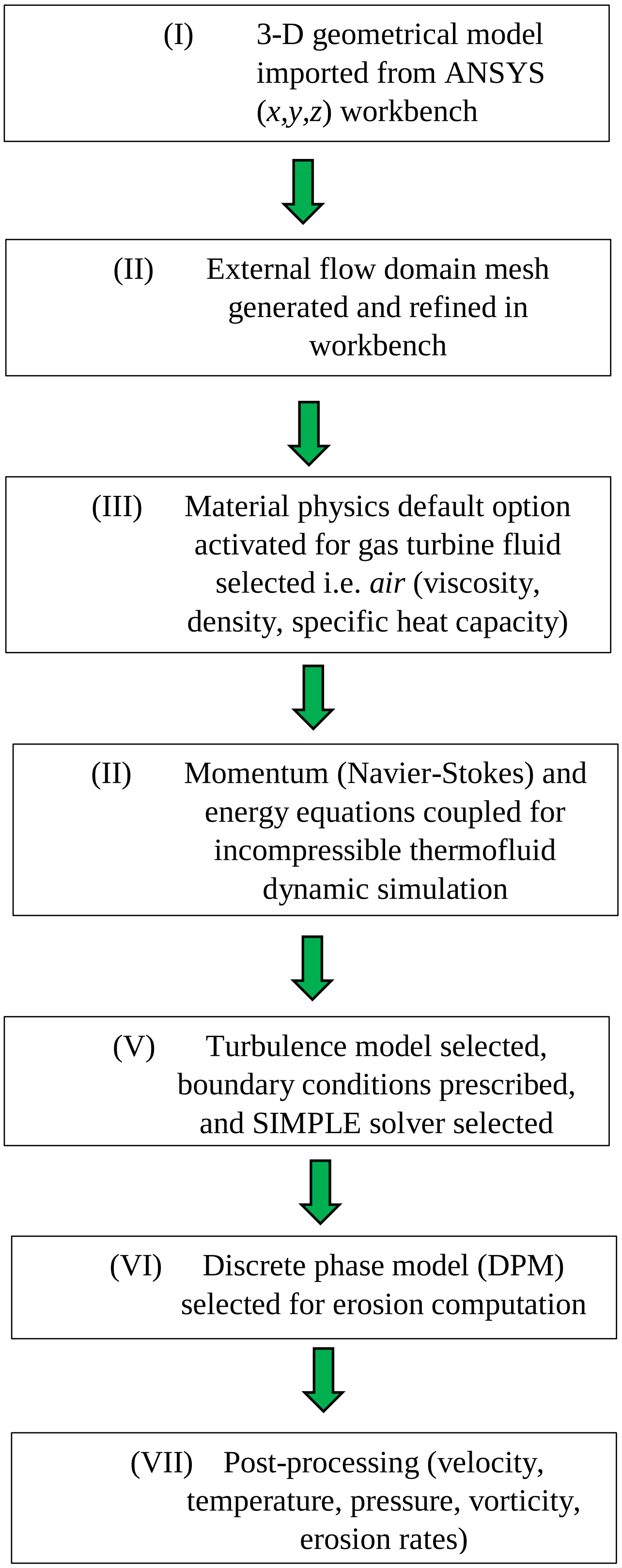

Figure 8. ANSYS FLUENT computational fluid dynamics procedure (CORRECTED FIGURE)

The **SIMPLE** (Semi-implicit pressure linked equation) is a very efficient numerical algorithm which computes the discretized momentum equations to generate an interim velocity. The face mass flux is then computed using the momentum interpolation method. The discretized continuity equation is solved to generate the pressure correction. Next the cell-central pressure and velocity are corrected and once convergence is attained the simulations are terminated. The turbulence calculations are linked to this procedure and further details are given in Daud et al., [28]. Similarly, the temperature values are computed by solving the energy balance equation and updated with corrected results.

3. COMPUTATIONAL RESULTS

3.1 Stress and Thermal Stress Analysis

In this section the results are outlined in 3 segments, the statical analysis, the thermal analysis and the fluent analysis. For the first 2 sections the results will be compared for each of the three cases i.e. double coated sample (Titanium and SiC ceramic) i.e. “three-layer model”, single coated sample (Titanium) sample i.e. two-layer model and finally the unprotected steel blade sample i.e. single layer model. Total deformation plots are shown in Figures 9-11.

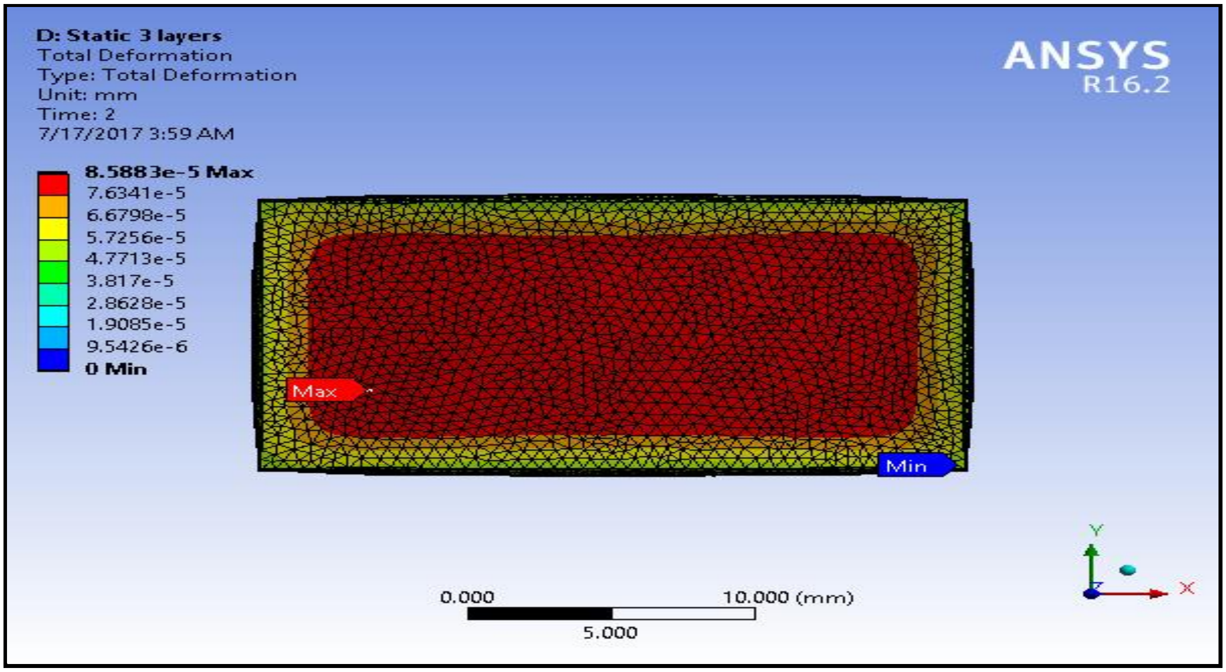

Figure 9. Total deformation results for three-layer model (steel + Titanium + SiC ceramic)

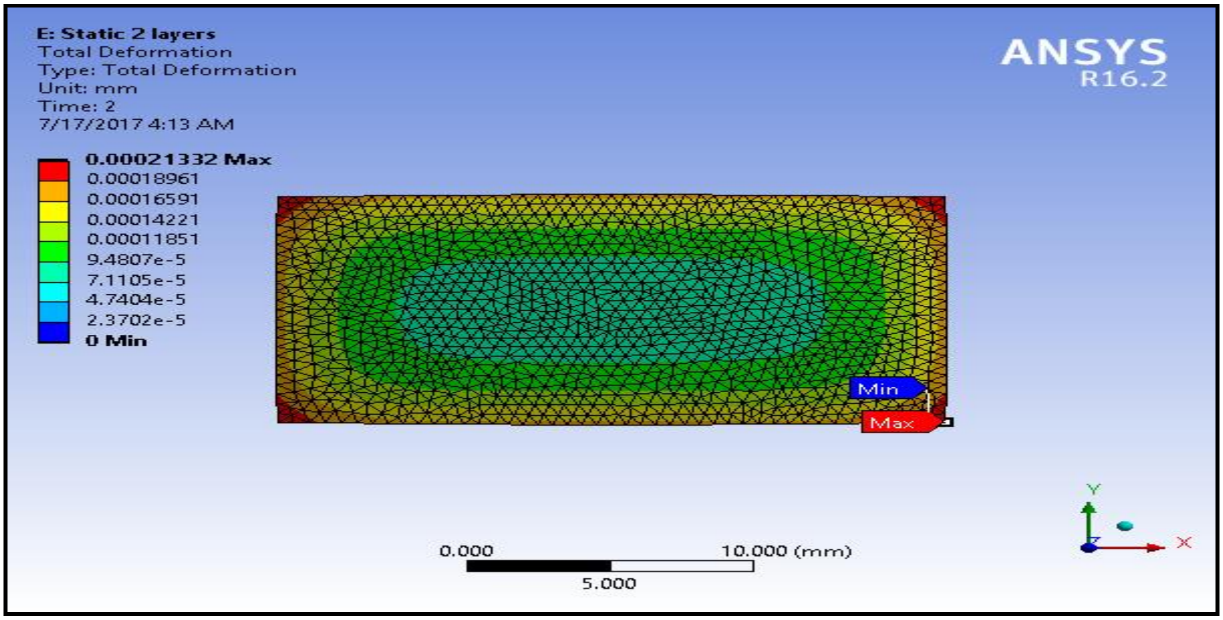

Figure 10. Total deformation results for two-layer model (steel + Titanium)

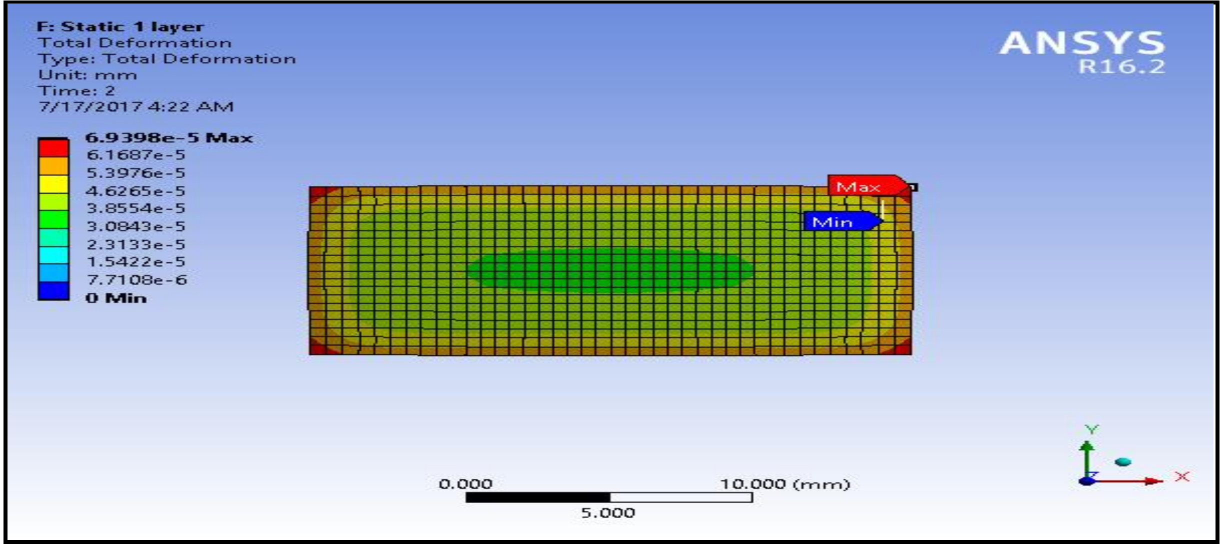

Figure 11. Total deformation results for one-layer model (steel)

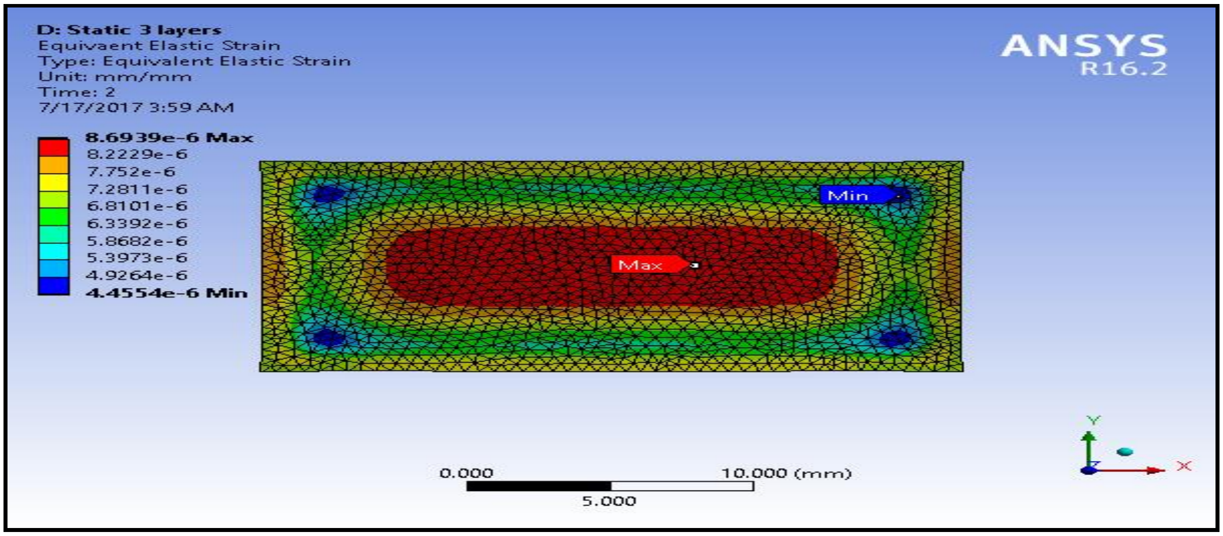

Figure 12. Equivalent elastic strain results for three-layer model (steel + Titanium + SiC ceramic)

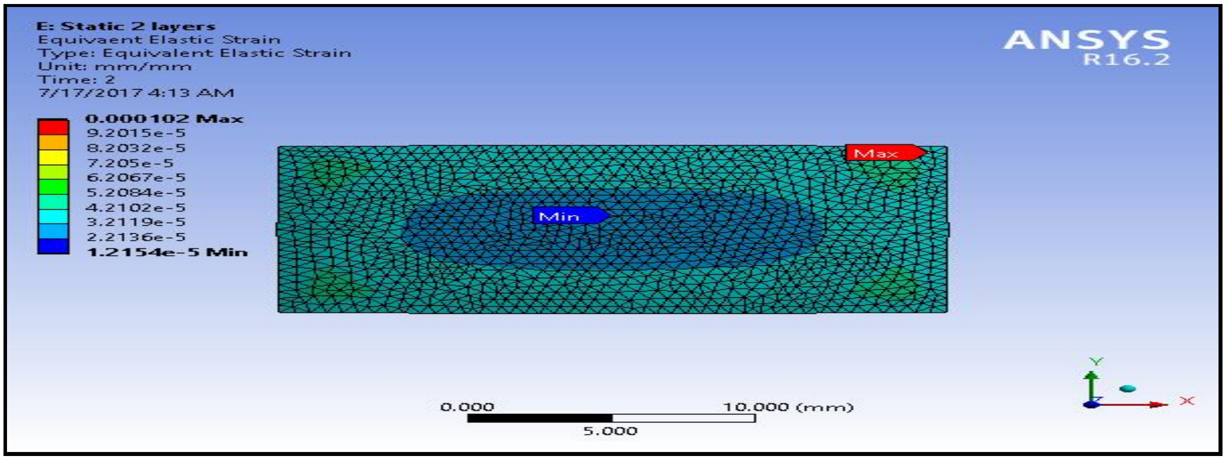

Figure 13. Equivalent elastic strain results for two-layer model (steel + Titanium)

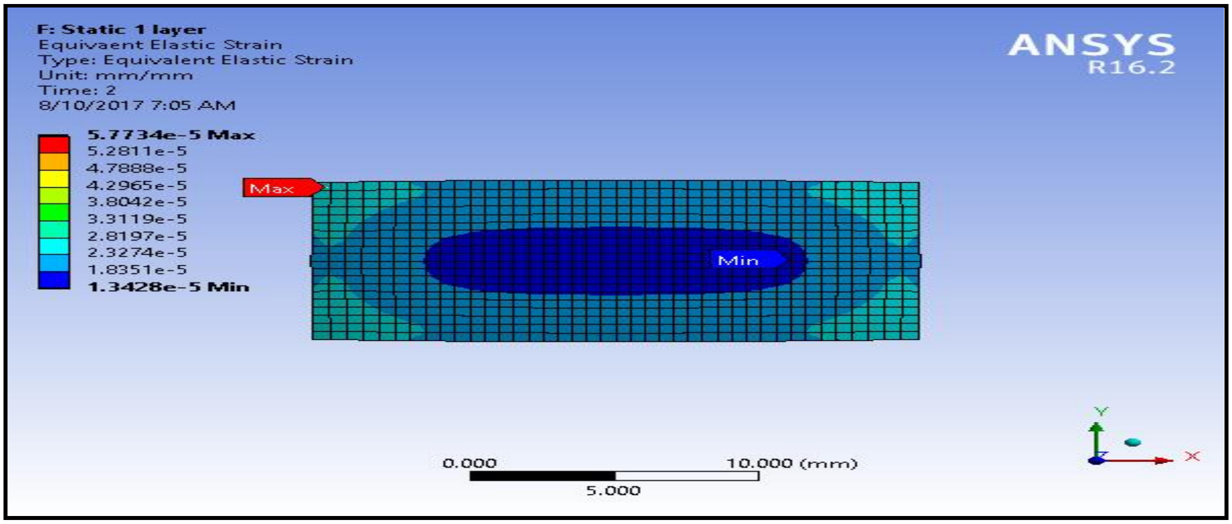

Figure 14. Equivalent elastic strain results for one-layer model (steel)

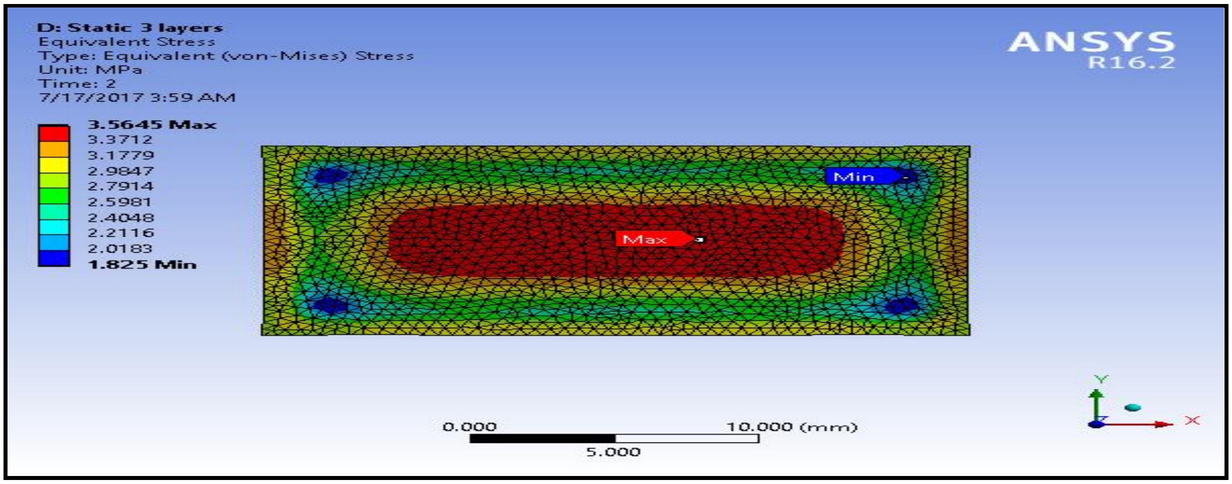

Figure 15. Equivalent stress plot for three-layer model (steel + Titanium + SiC ceramic)

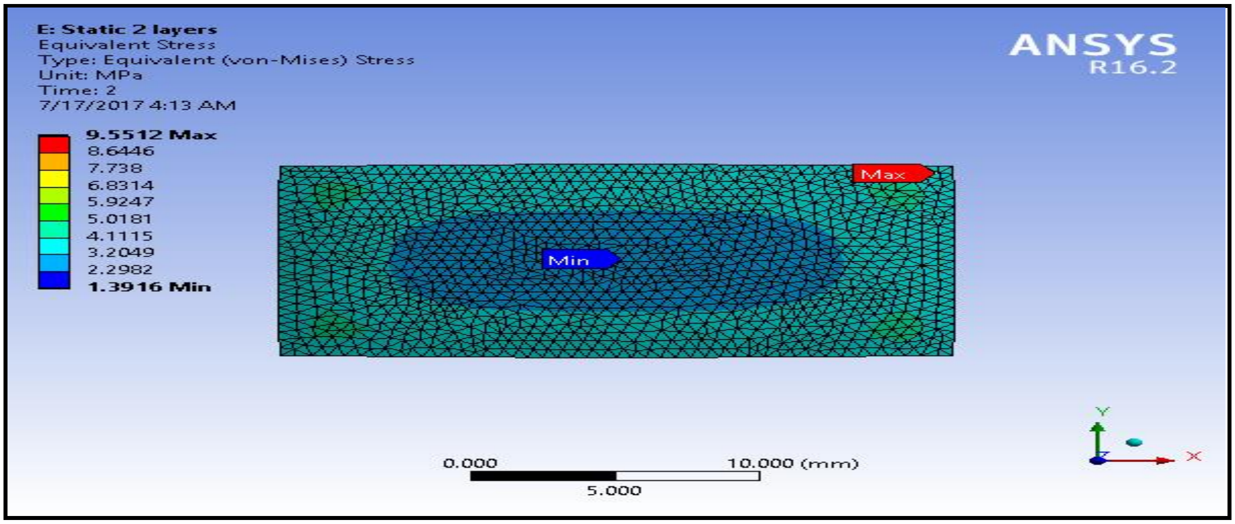

Figure 16. Equivalent stress plot for two-layer model (steel + Titanium)

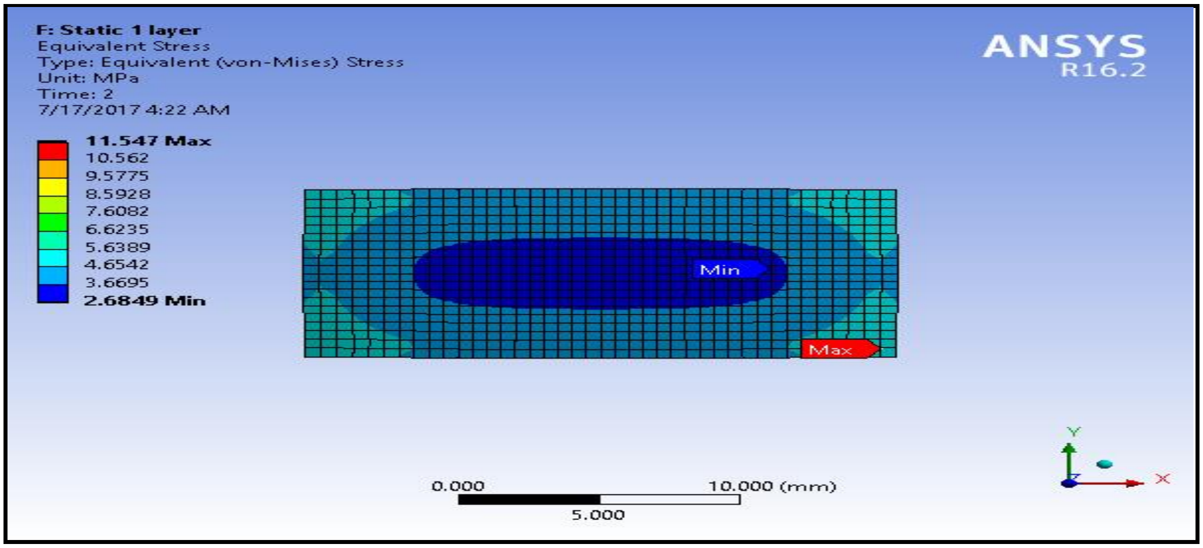

Figure 17. Equivalent stress plot for one-layer model (steel)

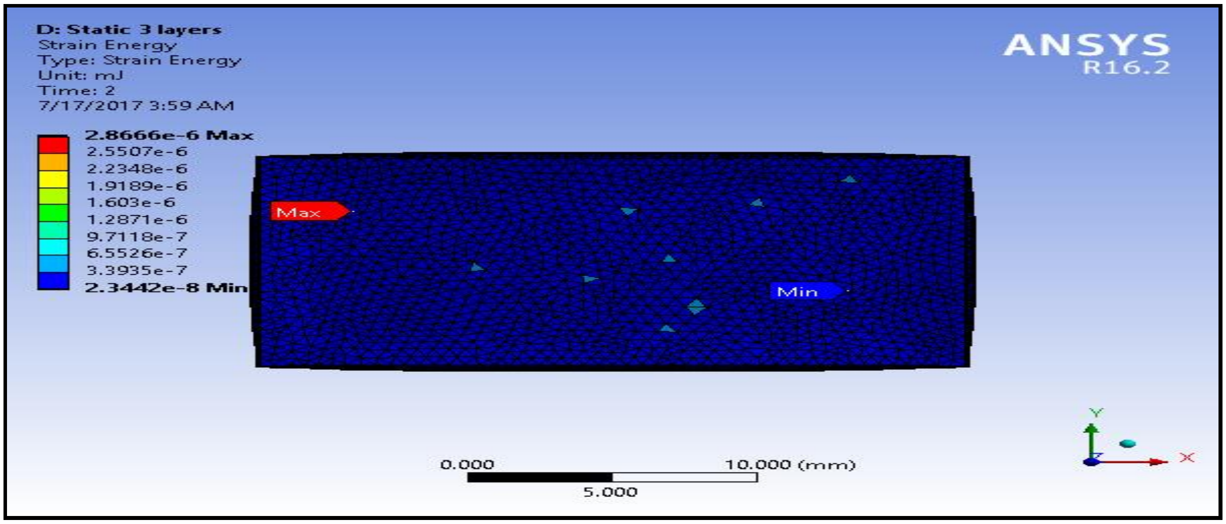

Figure 18. Strain energy distribution for three-layer model (steel + Titanium + SiC ceramic)

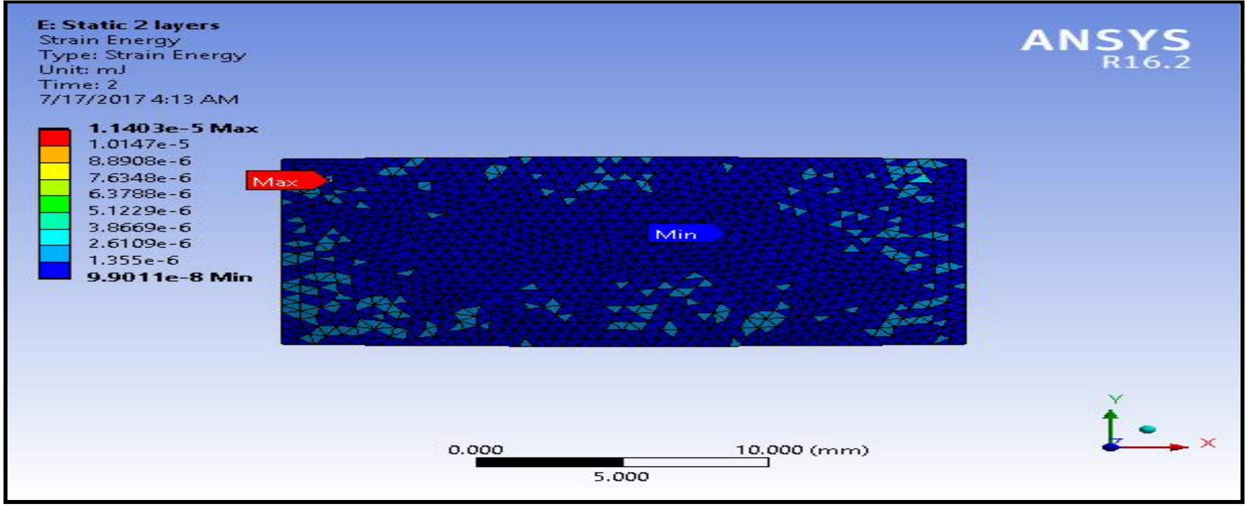

Figure 19. Strain energy distribution for two-layer model (steel + Titanium)

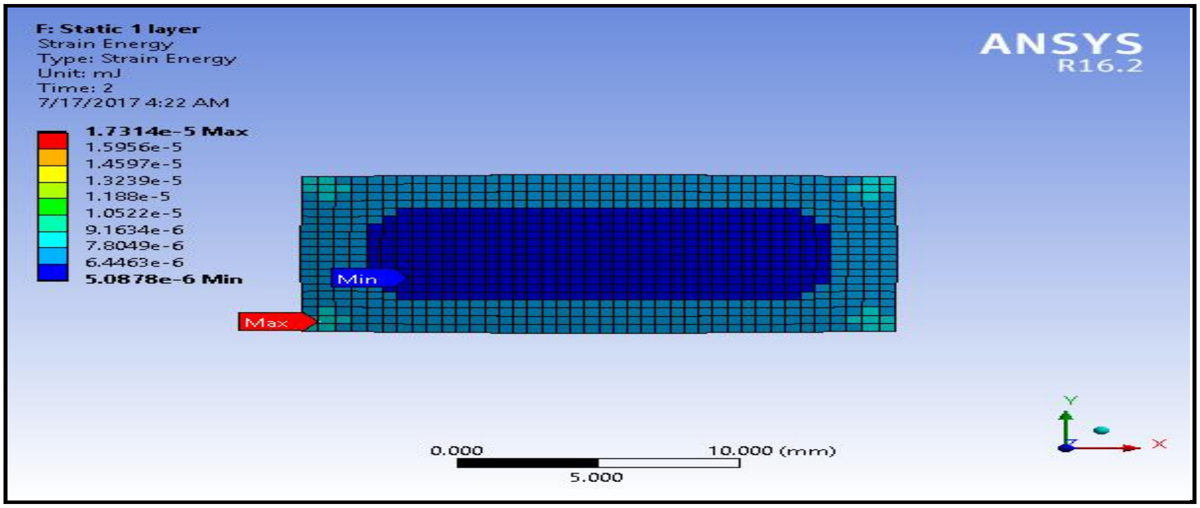

Figure 20. Strain energy distribution for one-layer model (steel)

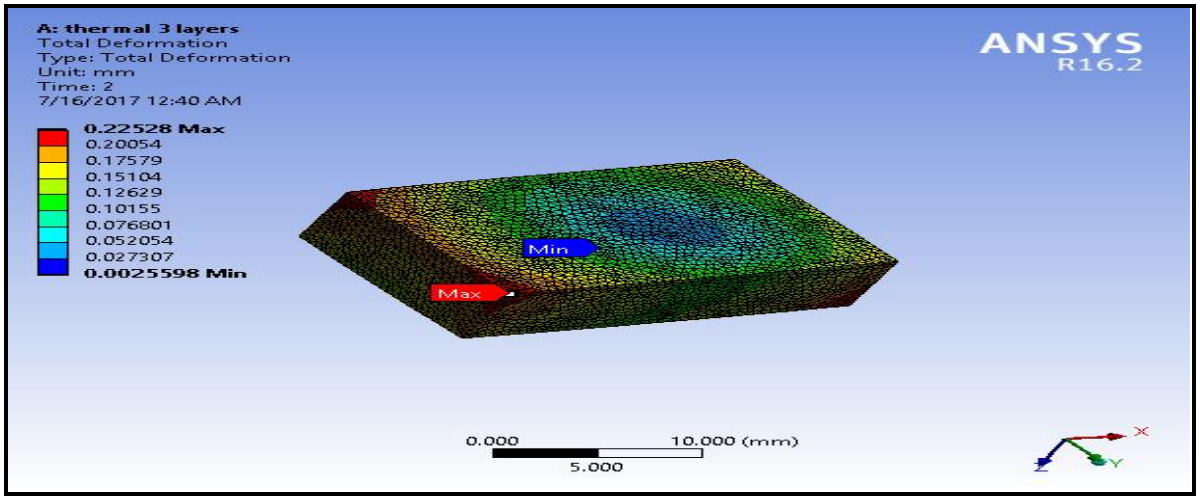

Figure 21. Total deformation for three-layer model (steel + Titanium + SiC ceramic) – thermal case

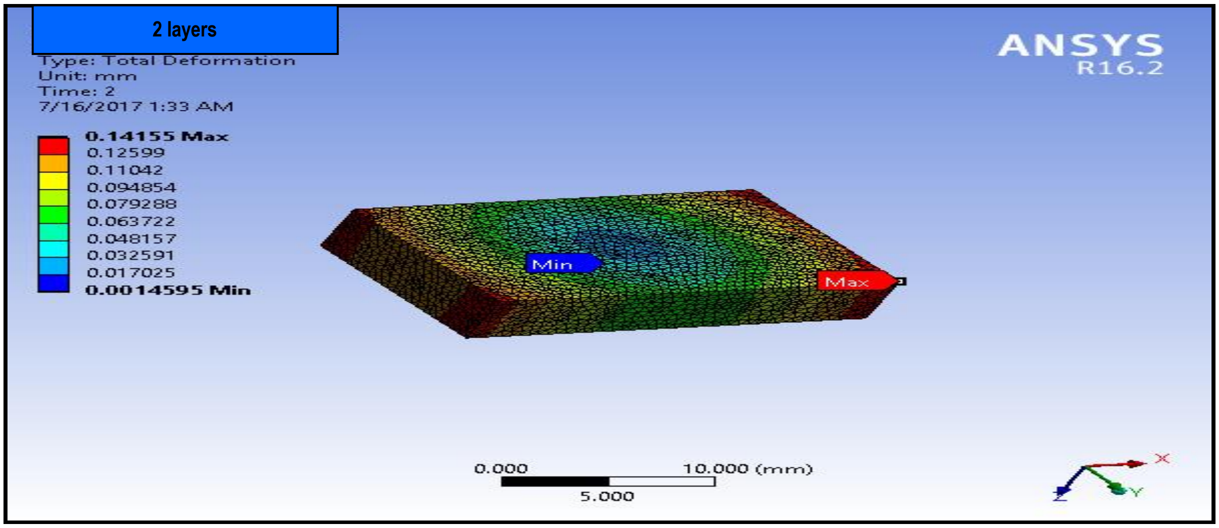

Figure 22. Total deformation for two-layer model (steel + Titanium) – thermal case

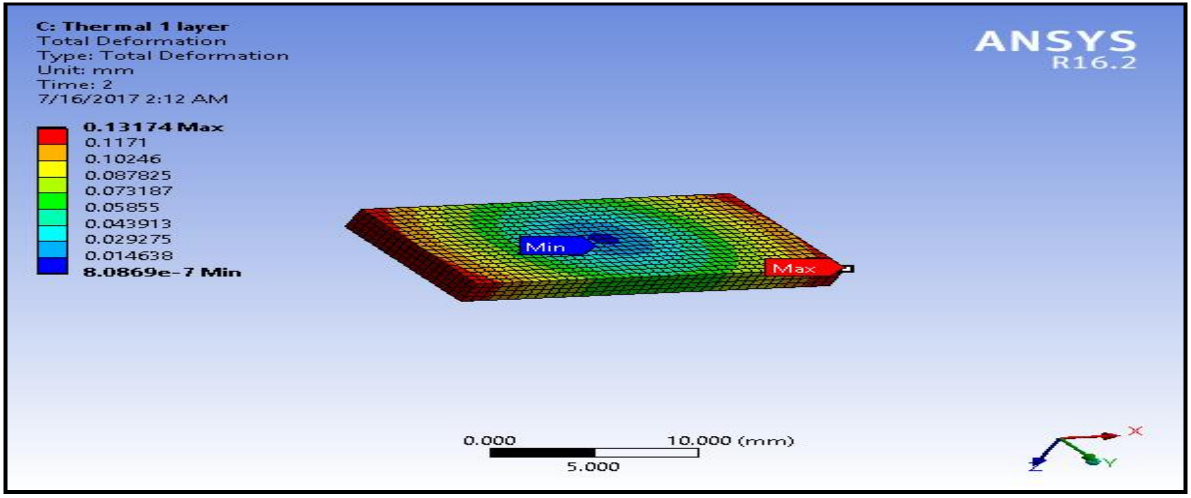

Figure 23. Total deformation for one-layer model (steel) – thermal case

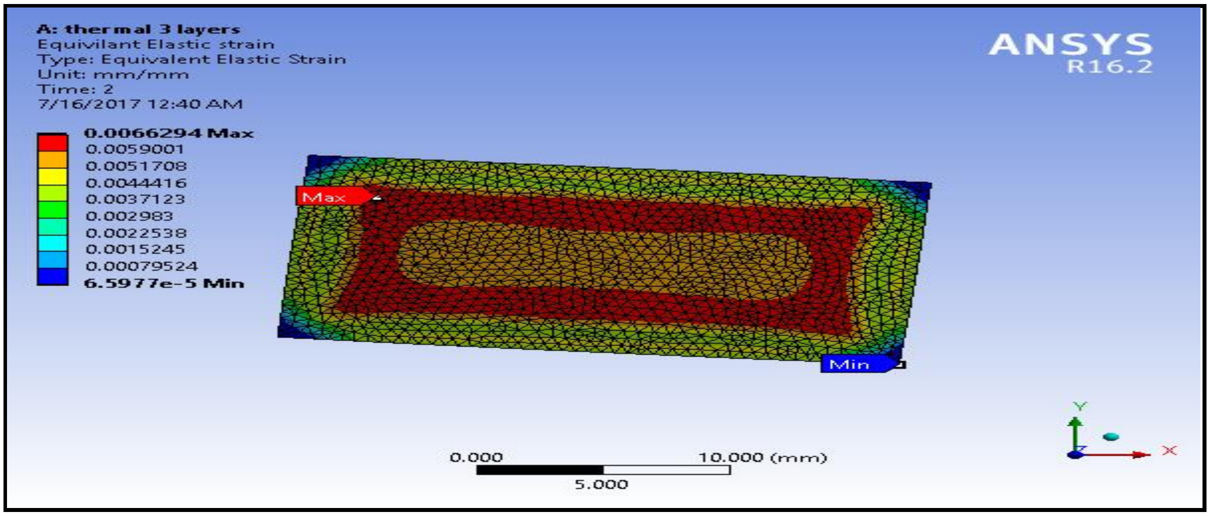

Figure 24. Equivalent elastic strain for three-layer model (steel + Titanium + SiC ceramic) – thermal case

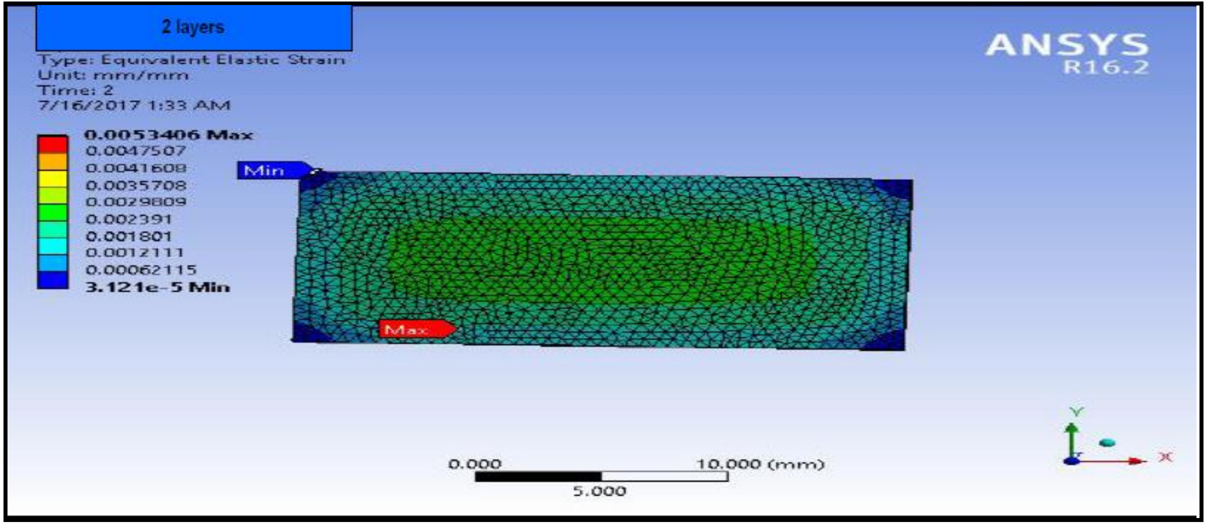

Figure 25. Equivalent elastic strain for two-layer model (steel + Titanium) – thermal case

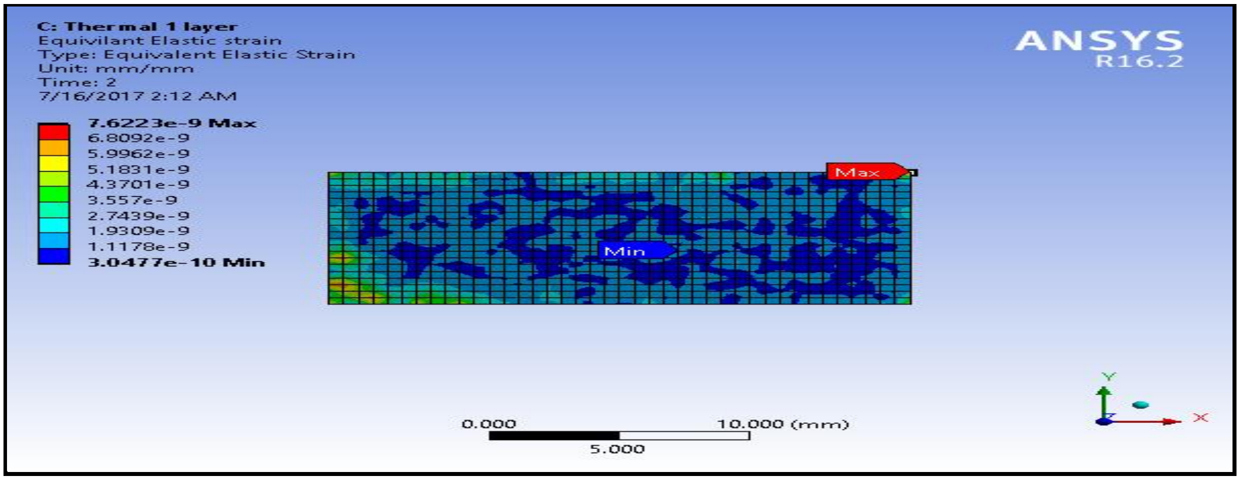

Figure 26. Equivalent elastic strain for one-layer model (steel) – thermal case

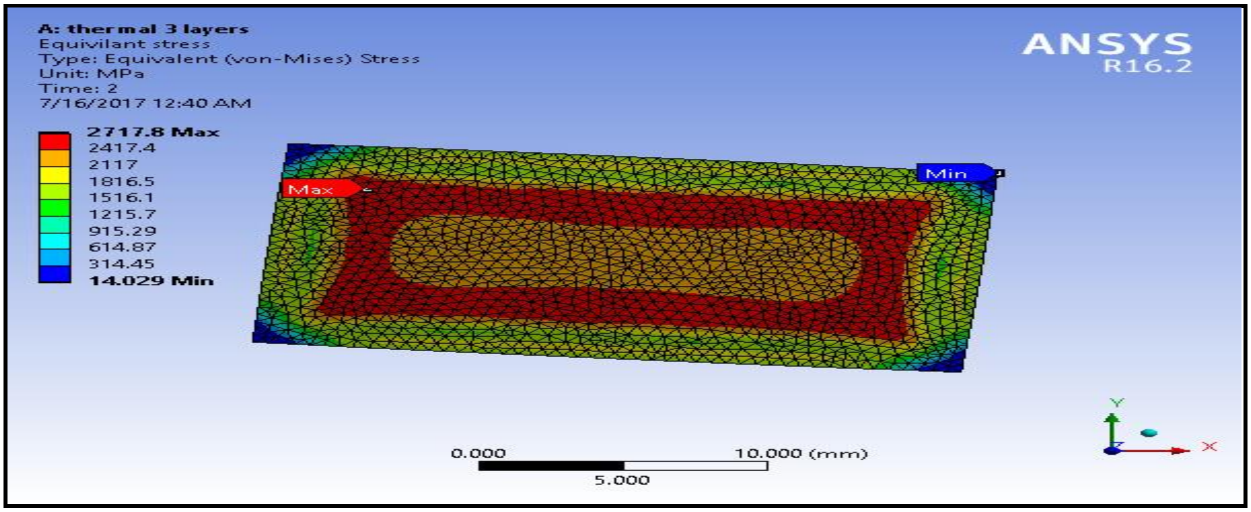

Figure 27. Equivalent elastic stress for three-layer model (steel + Titanium + SiC ceramic) – thermal case

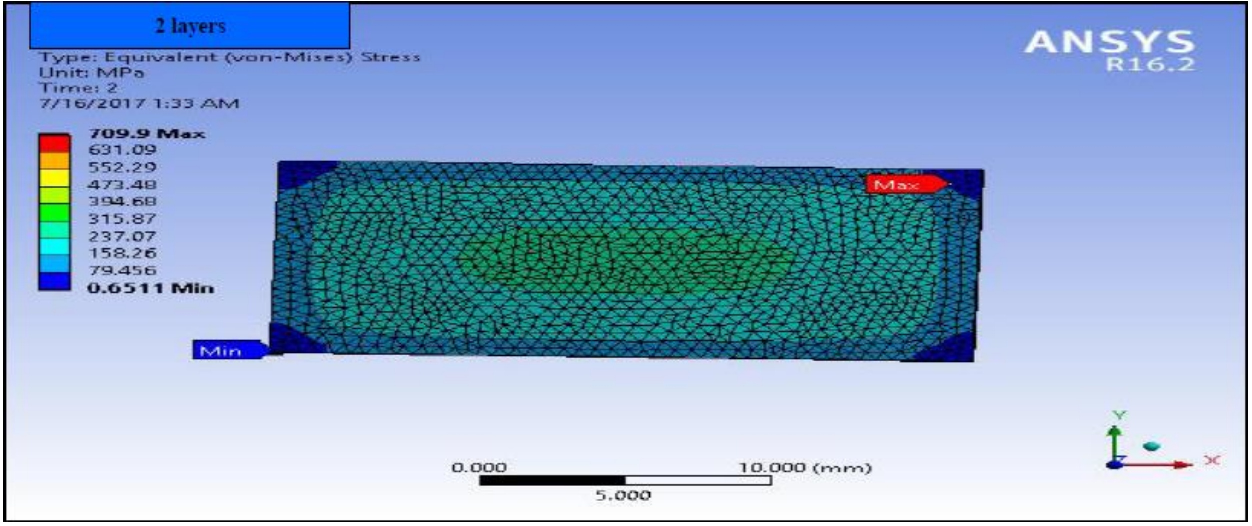

Figure 28. Equivalent elastic stress for two-layer model (steel + Titanium) – thermal case

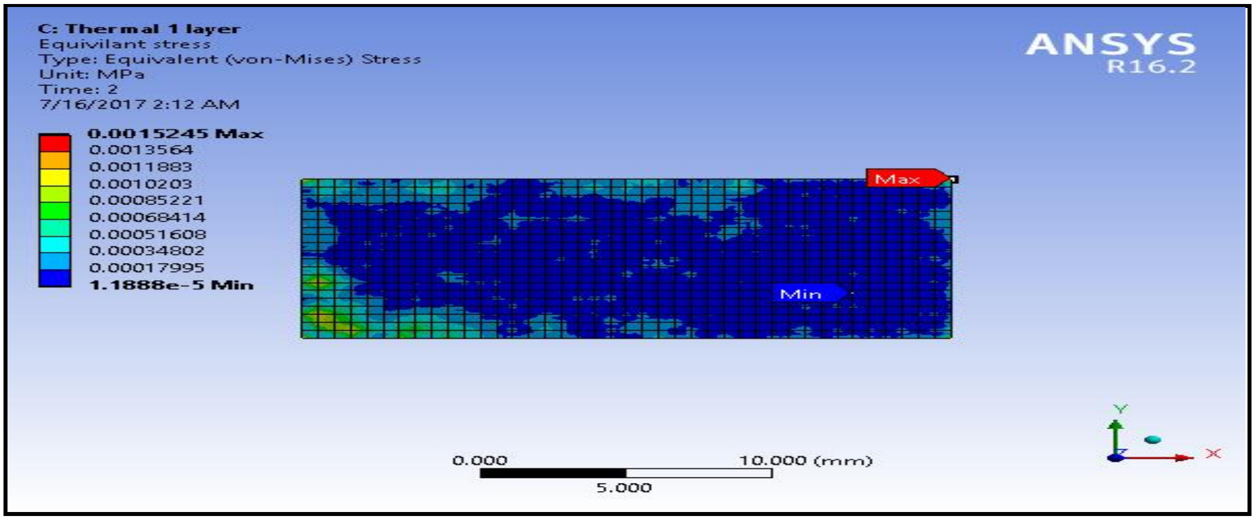

Figure 29. Equivalent elastic stress for one-layer model (steel) – thermal case

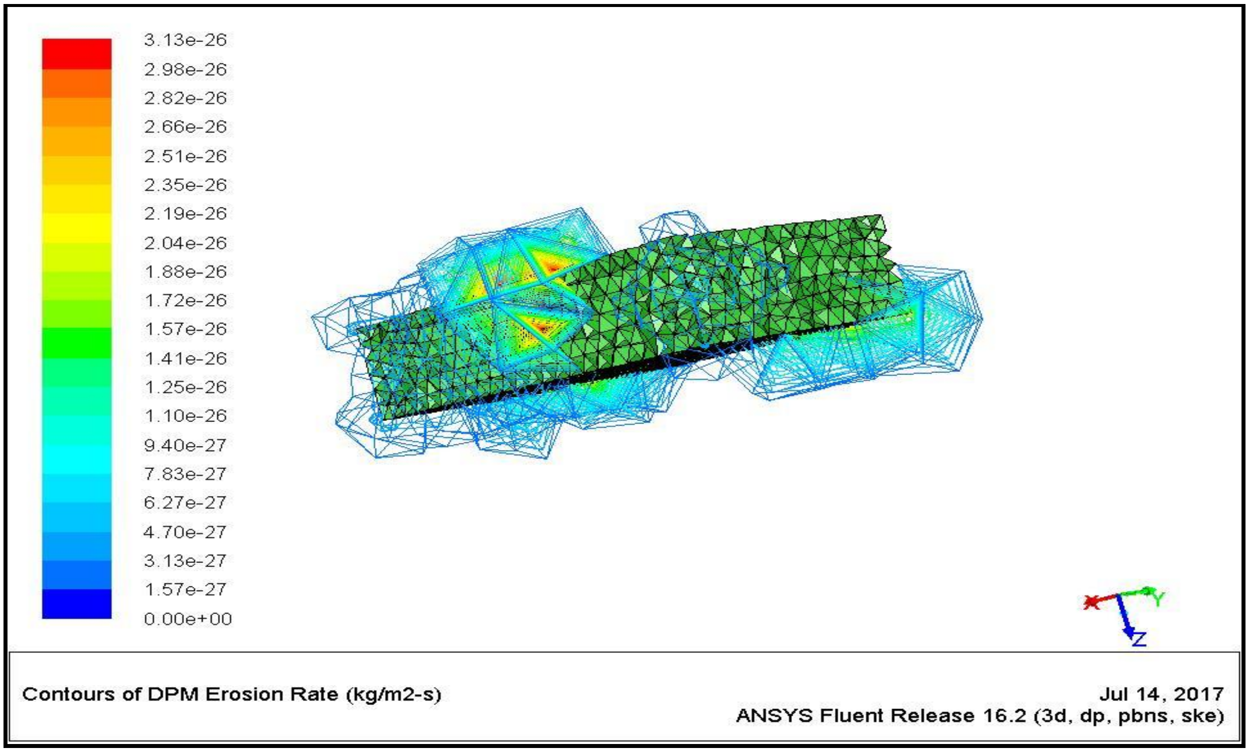

Figure 30. Erosion rates computed with DPM in ANSYS FLUENT

4. DISCUSSION

Figures 9-30 present extensive results for three types of analysis. These are respectively *static stress analysis* (Figures 9-20), *thermal stress analysis* (Figures (21-29)) and finally *CFD erosion simulation* (Figure. 30). In the first two sets of simulations (i.e. Figures 9-20 and Figures 21-29) we consider each of the coating cases in turn i.e. three-layer model (steel + Titanium + Silicon Carbide (SiC) ceramic), two-layer model (steel + Titanium) and the uncoated (steel) model. However, in the last analysis (CFD erosion i.e. Figure 30) only the three-layer model (steel + Titanium + Silicon Carbide (SiC) ceramic) is considered.

In both the *first* (static) and *second* (thermal stress) analysis, four elastic characteristics are considered- *total deformation, equivalent elastic strain, equivalent stress and strain energy distribution.* These four quantities require some clarification for readers not familiar with ANSYS or commercial finite element software. ANSYS [29] generates *displacements and stresses* as output in both elastic or inelastic (nonlinear) simulations. In displacement, it permits checking of deformation (displacement) in 3 directions viz., x, y and z. These are *directional deformations*. Total deformation is generally shown as "Mag" in ANSYS and gives an average overall deformation of the system as the square root of the sum of the squares of the directional deformations. In ANSYS the equivalent strains for the elastic (or other e.g. plastic, creep and thermal strains) are computed in postprocessing using the von Mises equation [32] which is known to be a function of appropriate component strain values and the effective Poisson's ratio. The von Mises equation is a measure of the "shear" strain in the material and does not account for the hydrostatic straining component. For example, strain values of $\varepsilon_x = \varepsilon_y = \varepsilon_z = 0.001$ yield an equivalent strain $\varepsilon_{eq} = 0.0$. The equivalent elastic strain is related to the equivalent elastic stress. Computation of equivalent total strain in ANSYS is only valid for proportional loading and is approximately valid for monotonic loading. *Strain energy is defined as the energy stored in a body due to deformation* and in ANSYS again this value is computed from stress and strain results. These versions of deformation and stress or strain provide *generalized overall magnitudes* of the quantities of interest in three-dimensional finite element stress analysis.

Figures 9-20 are discussed first. We therefore first consider the *non-thermal* scenario for total deformation in all three coating cases. Inspection of the two-dimensional face deformation contour surface plots indicates there is a significant variation in deformation with the three different combinations. Substantially higher deformations are computed in the three-layer model (dual Titanium and Silicon Carbide (SiC) ceramic coatings) as shown in Figure 9. The large red (high deformation) zone covers most of the steel model surface. The maximum deformation arises in the lower left quadrant towards the left edge. The minimal deformation is in the opposite quadrant closer to the right edge. With titanium coating added (Figure 10), the high deformation zone is eliminated in the major central area of the face. However small red zones re-emerge at the corners of the coated plate structure. The maximum deformation is observed in the lower quadrant corner vicinity and the minimum deformation is located in close proximity further upwards near the right edge. Concentric bands of progressively lower deformation (orange, yellow, light green, dark green, light blue) are witnessed as we move for the periphery to the central zone. Generally, a deformation gradient is achieved i.e. smoother deformation transition from the edges to the core, which is absent in the single layer steel model (where very narrow bands are confined to the outermost periphery of the structure). With the purely steel case (uncoated) there is an even more significant departure from the purely steel case. Much larger high deformation zones are computed at the corners and there is also a slightly higher deformation zone in the core region (Figures 11 and 10) compared with the two-layer model. The presence of a titanium coating therefore clearly suppresses deformation for the vast majority of the area of the loaded gas turbine surface. The great resilience of Titanium is therefore shown here. However only with the addition of ceramic coating are the *peak deformation zones* reduced at the edges (Figure

10) which are discontinuities and potential zones for failure. In Figure 11 it is also noteworthy that the minimum deformation migrates deep into the upper right quadrant edge as opposed to the two-layer model (Figure 10) where it (as discussed earlier) appears at the lower right quadrant edge. The maximum deformation location is also distinctly altered from figure. 9 (three-layer model) and figure 10 (two-layer model) as it is now computed at the upper right quadrant corner. The presence of ceramic in addition to Titanium coating layers (Figure 9) therefore, provides additional resistance to deformation of the surface of the structure as whole, although only Titanium (Figure 10) significantly suppresses high deformation in the central zone. An important achievement with the three-layer model (Figure 9) is that maximum deformation is further from any edge indicating that the potential for failure is lowered. Figures 12-14 depict the equivalent elastic strain plots for the three models studied. It is evident that the maximum strain is only computed in the core zone (far from the edge discontinuities) for the three-layered model (Figure 12) and the minimum elastic strain is located near the uppermost edge of the surface. However elastic strain values are quite high in the core area. For the two-layered model (Figure 13) the maximum strain location is pushed to the upper edge (right corner) and again for the single layer model it arises near the upper edge although it is displaced towards the left top corner. The dual and single layer models therefore do not achieve the desired effect i.e. they localize the maximum strains in the edge zones where failure is most likely to occur. The combination of titanium and silicon carbide ceramic is successful in avoiding this by restricting maximum elastic strain to the central zone which is the strongest and least likely to fail under loading. Figures 15-17 illustrate the equivalent elastic stress computational plots for the three coating layer cases. The three-layered model (Figure 15) produces a maximum stress in the core zone (central area) whereas this is displaced towards the upper and lower edges, respectively, for the two-layer model (Figure 16) and single layer (uncoated) model (Figure 17) with a strong orientation towards the right vertical edge (the minimum stress locations are always in the core area for these models whereas minimum stress is pushed into the upper edge corner zone for the three-layer model). This is undesirable again since the probability of failure is greatest at the edges. The amalgamation of a titanium coating layer and silicon carbide layer therefore produces more beneficial stress distributions and reduces the likelihood of structural degradation and failure at the edges. The strain energy distributions are shown in Figures 18-20 for the three model cases. Maximum strain energy is further into the surface area for the three-layer model (Figure 18) compared with the two-layer model (Figure 19) and single layer model (Figure 20) in which it is displaced progressively further towards the left vertical edge. A much more homogenous distribution of strain energy is noted in figure 17. Some variation and heterogeneity are computed for the two-layer

model (Figure 19); however, there is a significantly different pattern for the single layer model (Figure 20) which exhibits an outer periphery band of low strain and an inner oblate edged rectangular zone of minimum strain energy. The computations show good similarity with other single, two- and three-layered finite element models, for example Tavaresa et al., [33] and Shekeri et al., [34].

Figures 21-29 present computational visualizations for the i.e. three-layer model (steel + Titanium + Silicon Carbide (SiC) ceramic), two-layer model (steel + Titanium) and the uncoated (steel) model. For the simulations in Figures 21-23 we have shown the full body models (3-dimensional) rather than just the top surface two-dimensional distribution plots (as in Figures 9-20). The presence of heat significantly modifies the total deformation plots. Red (high deformation) zones are localized in all three cases at the left and right vertical cases; however, the zone of influence penetrates much deeper into the body for the single layer model (Figure 23), less-deeper with titanium coating (Figure 22) and is minimized with the dual ceramic and titanium coating (Figure 21). Much lower total deformation is also computed throughout the body of the structure in figure 21 indicating that the dual coating achieves the best performance overall. As corroborated by [35] there is clearly a non-uniform distribution of temperature at different locations of the coated steel specimen (hypothetical blade surface), which directly impacts on deformation field. Even though the analysis is thermally and elastically isotropic, there is still irregularity in the heat transferred via thermal conduction through the body of the material. Maximum deformation is observed at the bottom left corner of the upper surface in the three-layered model whereas it is confined to the bottom right corner for the two-layer and single layer models. Figures 24-26 illustrate the evolution in equivalent strain contour plots for the three different coating models examined. While lower strains are computed in Figure 26 (single layer model) the maximum strain is located near the edge. Higher strains are computed for the two-layer model (Figure 25) – however again with only titanium coating, the maximum stress is dangerously close to the lower edge. Only with the three-layer combined ceramic and titanium coating model (Figure 24) is the maximum equivalent strain pushed deeper towards the core central area. Here the desired effect of restricting high stresses to the strongest region of the gas turbine blade model is achieved whereas in the other two model's lower strains are produced in the core central zones. Unlike other studies e.g. Breitbach and Schubert [35], in the current study a conjugate heat transfer analysis with fully coupled thermal-stress calculation is conducted (i.e. the model is not decoupled as in many other studies). The thermal results indicate that strain state of the structural material adjacent to the coating interface is the controlling mechanism for the coating strains. Due to the non-uniform distribution of displacement, strain and stress in a real gas turbine blade, the regions located at the top and bottom sides tend to produce a maximum of displacement, with the occurrence of a bigger strain or stress, where *sub-critical cracks* preferentially form. The simulations confirm this trend and agree with the general findings in the literature of for example Cao et al., [2] and Fan et al., [3]. Figures 27-29 show the equivalent elastic stress contour plots for the three coating models. For the three-layer model (Figure 27) a similar distribution to the static case (Figure. 15) is observed indicating that the heat has the least impact on stress distribution when both ceramic and titanium coatings are combined. However significantly higher stresses are computed for the two-layer model and especially single layer model in figures 28, 29 compared with their non-thermal static analysis equivalent plots in Figures 16, 17. Higher stresses are also computed at the edge zones for the thermal cases of single and two-layer models compared with the static cases. Overall therefore the required protection is best provided by the ceramic-titanium-steel model confirming the excellent thermal protection barrier properties of both ceramics and titanium under high temperature loading scenarios.

Finally, some preliminary results of CFD analysis are given in Figure 30 for the erosion rates induced in the three-layer model as obtained by ANSYS FLUENT. Generally maximum erosion rates are confined to a local zone on the upper face of the three-layer system which is infact the sacrificial layer (ceramic coating). The titanium is not debonded or damaged which is essential for creating a buffer to the actual blade surface. However, the poor performance of ceramics (cracking, delamination, spalling) may be inhibited with improved nano-embedded coating particles and efforts in this direction are currently underway. Furthermore, we have provided material properties of blade substrate and coating layers for steel, titanium and silicon carbide ceramic in the appendix in Table 3. A more detailed CFD analysis is currently being conducted and will be reported imminently in a separate article. Owing to brevity, we have not included extensive CFD results here.

5. CONCLUSIONS

To simulate the thermal performance of coatings in high-temperature gas turbine blade protection, detailed finite element stress and computational fluid dynamics simulations of a 3-dimensional, 3-layered model of a test sample representing a typical gas turbine component scenario have been conducted. Structural steel is selected for the main inner layer (blade material), Titanium (Ti) alloy for the middle layer and Silicon Carbide (SiC) for the outermost layer. The model dimensions are 20 mm (width), 10 mm (height) and three 1mm deep layers. ANSYS software has been deployed to conduct three types of analysis- static structural, thermal stress analysis and also computational fluid dynamic erosion/corrosion analysis (via ANSYS FLUENT). The specified geometry which corresponds to corrosion test samples exactly is discretized using a body-sizing meshing approach, comprising mainly of tetrahedron cells. Refinements have been localized at the connection points between the layers (interfaces) to concentrate the focus towards the static effects dissipated between them. A detailed grid independence study has been executed to confirm the accuracy of the selected mesh densities. To recreate gas turbine scenarios, in the stress analysis simulations, static loading and thermal environment conditions of up to 1000 N and above 1000 K have been imposed. ANSYS FLUENT simulation was conducted to study the effect of corrosion on the model under similar thermal conditions. This required significant modification of the mesh to accommodate for the size of the air particles leading to the erosion of the structure. This refinement was executed in the solver component of the simulation to avoid altering the main mesh of the structure and to mitigate errors. The momentum and energy equations were efficiently solved, and the viscous heating option was applied to represent improved thermal physics of heat transfer between the layers of the structures. The discrete phase model (DPM**)** in ANSYS FLUENT was employed which allows for the injection of continuous uniform air particles onto the model, thereby enabling an option for calculating the erosion factor caused by hot air injection (particles prescribed 5 m/s velocity and 1273.15 K). Extensive visualization of results has been provided. The simulations reveal interesting features associated with coating response to realistic gas turbine loading conditions including significantly different stress/strain/deformation/strain energy concentrations with different coatings. Generally, the ANSYS stress analysis and CFD simulations have proven to be robust and provide a good insight into the different protection performances achieved by using different coatings on a gas turbine steel blade in a high-temperature corrosive environment. Ceramic (silicon carbide) when combined with titanium clearly provide good thermal protection; however, the ceramic coating is susceptible to cracking and the titanium coating layer on its own achieves significant thermal resistance. Maximum stress/deformation/strain zones are pushed further into the body of the glade model with the three-layer design which provides better protection and circumvents the possibility of crack initiation and propagation which is associated with gas turbine failure. This performance is not achieved with the pure steel design or the dual titanium-steel designs. While lower strains are computed for the single layer model (thermal case), the maximum strain is located near the edge. Higher strains are computed for the two-layer model than the single layer model (thermal case) however even with titanium only present as a coating the maximum equivalent elastic strain is still dangerously close to the lower edge. Only with the three-layer combined ceramic and titanium coating model is the maximum equivalent strain pushed deeper towards the core central area. Here the desired effect of restricting high stresses to the strongest region of the gas turbine blade model is achieved, whereas in the other two models, lower strains are produced in the core central zones. The present simulation involves a conjugate heat transfer analysis with fully coupled thermal-stress calculation is conducted (i.e. the model is not decoupled as in many other studies). The thermal results indicate that strain state of the structural material adjacent to the coating interface is *the controlling mechanism* for the coating strains. Due to the non-uniform distribution of displacement, strain and stress in a real gas turbine blade, the regions located at the top and bottom sides tend to produce a maximum of displacement, with the occurrence of a bigger strain or stress, where *sub-critical cracks* preferentially form. The current study has provided a good foundation for more refined computational analysis and central to this is the inclusion of an actual 3-dimensional skewed blade geometry. Furthermore, the ceramic may be enhanced in performance by embedding nano-particles which create better bonding to the lower substrate (titanium) and mitigate delamination and crack penetration through the ceramic layer. Efforts to develop more sophisticated thermal barrier coating simulations in these directions (in addition to verification with experimental testing and considering alternative turbulence models [36]) are presently underway and will be communicated imminently [37, 38].

Acknowledgements

This research did not receive any specific grant from funding agencies in the public, commercial, or not- for profit sectors. The authors are extremely grateful to the reviewers for their comments which have improved the present article significantly.

Compliance with Ethical Standards

The ethical standards are considered in writing this paper. The authors have no conflict of interest with anybody or any organizations/companies.

REFERENCES

[1] Gleeson B (2006) Thermal barrier coatings for aero-engine applications, AIAA J. Propulsion and Power, 22:375-383.

[2] Cao XQ, Vassen R, Stoever D (2004) Ceramic materials for thermal barrier coatings, J Euro Ceramic Soc, 24:1–10.

[3] Fan X, Jiang W, Li J, Suo T, Wang TJ, Xu R (2014) Numerical study on interfacial delamination of thermal barrier coatings with multiple separations, Surface and Coatings Tech, 244:117–122.

[4] Ghasemi R, Shoja-Razavi R, Mozafarinia R, Jamali H (2013) Comparison of microstructure and mechanical properties of plasma-sprayed nanostructured and conventional stabilized zirconia thermal barrier coatings, Ceramics Int, 39:8805–8813.

[5] Padture NP, Gell M, E. H. Jordan EH (2002) Thermal barrier coatings for gas-turbine engine applications, Science, 296:280–284.

[6] Echsler H, Renusch D, Schutze M (2004) Bond coat oxidation and its significance for life expectancy of thermal barrier coating systems, Mat. Sci. Tech, 20:307-318.

[7] Patnaik PC, Elder JE, Thamburaj R (1988) Degradation of aluminide coated directionally solidified superalloy turbine blades in an aero gas turbine engine, Superalloys (Edited by Reichman, S., Duhl, D.N., Maurer, G., Antolovich, S. and Lund, C.,). The Metallurgical Society, USA.

[8] Mévrel R (1989) State of the art on high-temperature corrosion-resistant coatings, Mat. Sci. Eng. A, 120:13-24.

[9] Yoshiba M (1993) Effect of hot corrosion on the mechanical performances of superalloys and coating systems, Corros. Sci, 35:1115–1124.

[10] Yoshiba M, Abe K, Aranami T, Harada Y (1996) High-temperature oxidation and hot corrosion behavior of two kinds of thermal barrier coating systems for advanced gas turbines, J Thermal Spray Tech, 5:259–268.

[11] Bai CY, Luo YJ, Koo CH (2004) Improvement of high temperature oxidation and corrosion resistance of superalloy IN-738LC by pack cementation, Surface and Coatings Tech, 183: 74–88.

[12] Koo CH, Bai CY, Luo YJ (2004) The structure and high temperature corrosion behavior of pack aluminized coatings on superalloy IN-738LC, Mat. Chem. Phys, 86:258–268.

[13] Sumner J, Encinas-Oropesa A, Simms NJ, Oakey JE (2013) High temperature oxidation and corrosion of gas turbine materials in burner rig exposures, Mat. Sci. Tech, 29(7): 813-821.

[14] Oksa M, Metsajoki J (2015) Optimizing NiCr and FeCr HVOF coating structures for high temperature corrosion protection applications, J Thermal Spray Tech, 24:436–453.

[15] Khan MA, Sundararajan S, Natarajan S, Pad P, Mohandas E (2014) Oxidation and hot corrosion behavior of nickel-based superalloy for gas turbine applications, Mat. Manuf. Procs, 29:832-839.

[16] Bäker M (2012) Finite element simulation of interface cracks in thermal barrier coatings, Comput Mat Sci, 64:79-83.

[17] Chen X (2003) Failure mechanisms of thermal barrier coatings at high temperature, ASME 2003 Int. Mech. Eng. Congress and Exposition., USA.

[18] Yang L, Liu QX, Zhou YC, Mao WG, Lu C (2014) Finite element simulation on thermal fatigue of a turbine blade with thermal barrier coatings, J Mat Sci Tech, 30:371-380.

[19] Mohamed H (2013) Finite element analysis implementation of thermal barrier coating lifetime prediction methods, Master of Science Dissertation, University of Pittsburgh, USA.

[20] Fan X, Xu R, Wang TJ (2014) Interfacial delamination of double-ceramic-layer thermal barrier coating system, Ceramics Int, 40:13793–13802.

[21] Xu R (2014) Interfacial fracture mechanism associated with mixed oxides growth in thermal barrier coating system, Surface and Coatings Tech, 253:139-147.

[22] Gupta M, Curry N, Nylén P, Markocsan N, Vaßen R (2013) Design of next generation thermal barrier coatings-Experiments and modelling, Surface and Coatings Tech, 220: 20-26.

[23] Busso EP, Lin J, Sakurai S, Nakayama M (2001) A mechanistic study of oxidation-induced degradation in a plasma-sprayed thermal barrier coating system. part I: model formulation, Acta Mater, 49:1515-1528.

[24] Zhu W (2017) Modeling and simulation of the temperature and stress fields in a 3D turbine blade coated with thermal barrier coatings, Surface and Coatings Tech, 315:443-453.

[25] Tang WZ, Yang L, Zhu W, Zhou YC, Guo WC, Lu C (2016) Numerical simulation of temperature distribution and thermal-stress field in a turbine blade with multilayer-structure TBCs by a fluid–solid coupling method, J Mat Sci Tech, 32:452-458.

[26] Sadowski T, Golewski P (2011) Multidisciplinary analysis of the operational temperature increase of turbine blades in combustion engines by application of the ceramic thermal barrier coatings, Comput Mat Sci, 50:1326-1335.

[27] Daud HA, Li Q, Anwar Bég O, Ghani SAA (2011) Numerical investigations of wall-bounded turbulence, Proc IMechE Part C: J Mech Eng Sci, 225:1163-1174.

[28] Daud HA, Li Q, Anwar Bég O, Ghani SAA (2010) CFD modeling of blowing ratio effects on 3-D skewed gas turbine film cooling, 11th Int. Conf. Advanced Computational Methods and Experimental Measurements in Heat Transfer, Tallinn, Estonia.

[29] ANSYS User Manual version 16.2(2015) Swanson Analysis Systems, Pennsylvania, USA.

[30] ANSYS FLUENT Theory Guide version 16.2 (2015) Swanson Analysis Systems, Pennsylvania, USA.

[31] Kadir A(2017) Corrosion testing of steel, titanium coated steel and titanium-silicon carbide coated steel samples in hot corrosive environments: Technical Report. Aeronautical and Mechanical Engineering, University of Salford, UK.

[32] Bathe KJ (1996) Finite Element Procedures. Prentice-Hall, USA.

[33] Tavaresa CJ, Reboutaa L, Andritschkya M, Ramos S (1999) Mechanical characterization of TiN/ZrN multi-layered coatings, J Mat Procs Tech, 92/93:177-183.

[34] Shakeri M, Sadough A, Ahmadi SR (2008) Elastic stress analysis of bi-layered isotropic coatings and substrate subjected to line scratch indentation, J Mat Procs Tech, 196:213–221.

[35] Breitbach G, Schubert F (2004) A contribution to stress prediction in coatings for gas turbine blades, Archive of Appl Mech, 73(9/10):682–689.

[36] Jeyalaxmi PS, Kalivarathan G (2013) CFD analysis of flow characteristics in a gas turbine- a viable approach to predict the turbulence, Int J Mech Eng Tech, 4(2):39-46.

[37] Kadir A, Anwar Bég O, El Gendy M, Bég TA, Shamshuddin MD (2019) Further CFD-FEA computation of thermal corrosion-erosion in multi-layered gas turbine skewed blade coatings with nano-doping of upper ceramic barriers, **In Preparation**.

[38] Kadir A, Anwar Bég O, El Gendy M, Bég TA, Shamshuddin MD (2019) Coupled CFD-FEA thermal corrosion-erosion simulations of multi-layered gas turbine skewed blade coatings, **In Preparation**.

APPENDIX

TABLE 3: Material properties of blade substrate and coating layers

Property	**Steel**	**Titanium**	**Silicon Carbide Ceramic**
Young Modulus	200 GPa	100 GPa	450 GPa
Poisson Ratio	0.28	0.30	0.19
Density	7850 kg/m^3	4500 kg/m^3	3200 kg/m^3
Thermal conductivity	50 W/mK	20 W/mK	175 W/mK